

# FINAL REPORT

**Agenda 2020 Research Area(s):** **Energy Performance,**  
Area 1: New Approaches to Drying and Water Removal

**Project Title:** ACOUSTIC FORMING FOR ENHANCED DEWATERING AND FORMATION

**Date of Report:** November 2, 2007

**Recipient:** Institute of Paper Science and Technology at Georgia Tech.  
500 Tenth St., NW; Atlanta, GA 30332-0620

**Award Number:** DE-FC07-02ID14267

**Contact:** Cyrus K. Aidun, PI

**Principal Investigator:** Cyrus K. Aidun,  
Professor,  
G. W. Woodruff School of Mechanical Engineering  
Georgia Institute of Technology  
500 10th St. NW, Atlanta, GA 30332-0620,  
(404) 894-6645, Fax 4778, [cyrus.aidun@me.gatech.edu](mailto:cyrus.aidun@me.gatech.edu),  
Georgia 5th Congressional District.

## **ABSTRACT and key words:**

The next generation of forming elements based on acoustic excitation to increase drainage and enhances formation both with on-line control and profiling capabilities has been investigated in this project. The system can be designed and optimized based on the fundamental experimental and computational analysis and investigation of acoustic waves in a fiber suspension flow and interaction with the forming wire.

**PROJECT TITLE:****ACOUSTIC FORMING FOR ENHANCED DEWATERING AND FORMATION**

**PRINCIPAL INVESTIGATOR:** Cyrus K. Aidun, Professor, School of Mechanical Engineering, Georgia Institute of Technology, 500 10th St. NW, Atlanta, GA 30332-0620, (404) 894-6645, Fax 4778, [cyrus.aidun@me.gatech.edu](mailto:cyrus.aidun@me.gatech.edu), Georgia 5th Congressional District.

**RESEARCH AREA(S) IN THE SOLICITATION TO WHICH THIS WORK IS FOCUSED:** ENERGY PERFORMANCE, Area 1: New Approaches to Drying and Water Removal

**I. Executive Summary**

When ultrasonic waves are applied to pulp fibers in a liquid suspension, the fibers move away from the source due to the acoustic force acting on the fibers. The acoustic force consists of three major forcing mechanisms acting on a fiber. These are acoustic radiation, acoustic streaming, and capitation bubble-induced force. These mechanisms are inter-dependent and nonlinear as well as frequency-dependent. It is the combination of all three forces that contributes to the manipulation of pulp fibers suspended in liquid. In this project we use this effect at the early stages of the forming table to generate controlled normal force on the fiber mat in the forming section to: (a) re-fluidize the fibers in the fiber mat to increase the drainage rate, (b) generate controlled activity on the forming wire to enhance formation, and (c) through sectional excitation, profile the sheet for more uniform moisture profile. The results have had limited success, as a large portion of the acoustic energy is dampened while crossing the porous wire. We have done substantial evaluation of acoustic transmission through the actual forming wires and have compiled a substantial data set from the experiments, as presented in the appendix. Through this project we have been able to develop a technology for enhanced dewatering and formation improvement in some grades of specialty paper where the value of the final product is large enough for a favorable cost-benefit process.

**II. Introduction**

In the forming section, foils and suction boxes are used for dewatering of the pulp suspension delivered from the headbox. As soon as the forming jet impinges on the forming board, a layer of concentrated fiber mat forms on the forming wire. It has been demonstrated that by re-fluidizing the fiber mat at the early stages of the forming table, the dewatering rate increases resulting in additional drainage capacity along the same length of the forming section. Furthermore, it is demonstrated that this action enhances formation of the sheet by generating additional activity on the wire with benefits in quality and fiber savings (1). This application is currently limited to the use of undulating foils on slow speed machines. Although effective, there is lack of control on

the current system once the foils are placed in the forming section. These limitations make the current technology to be effective only from time to time depending on the process conditions. Replacing the undulating foils with the acoustically excited foils has the advantage of superior control and on-line optimization capability for any given grade or process condition.

Impedance matching between the acoustic transducer, the forming wire and the fiber mat is critical to the success of this technique. There is a fundamental impedance mismatch between the three components and the interaction between the three is driven by acoustic frequency and intensity, wire wetting (2, 3), wire weave (4) and fiber geometry (5). This highly complex and non-linear interaction has been investigated experimentally (see appendix). This report presents the results of a series of experiments to quantify the effect of high intensity ultrasound on a wood fiber mat in water. The results provide information on power intensity and pulse duration. Extensive experiments have been carried out to determine the interaction of acoustic waves with the commercial forming wires, as outlined in the appendix.

### **III. Method**

Results from earlier work indicate that the acoustic pressure exerted by a transducer on an absorber in the near field, 5-15 cm from the transducer face, increases exponentially with decreasing distance from the face and is at a maximum at a transducer frequency of 150 kHz. Thus for these tests the setup is confined to 150 kHz transducer mounted immediately beneath the forming wire.

A clear Plexiglas test cell was constructed with a 5 cm by 10 cm rectangular 150 kHz Sonic Concepts hydro-acoustic transducer mounted at the bottom. The cell was filled with plain tap water and the top surface was left open to the air. A fiber mat was formed by moving a 5 cm by 10 cm forming wire sample vertically through a suspension of softwood pulp resulting in a mat about 1 mm thick resting on top of the wire. The wire was placed at the bottom of the water filled cell, resting on the transducer surface, and tacked to the cell wall around its edges. A sequence of four identical acoustic pulses, triggered at one second apart, was emitted beneath the wire and the resulting fiber mat disruption was recorded using a Kodak Model 1000 HRC high speed digital video camera at 250 frames per second. Pulse duration was varied between 30, 60 and 90 milliseconds to simulate changes in wire speed or transducer size, and thus residence time of the fibers above the emitter on a paper machine, and transducer power input were varied from 2 to 10 Watts per square centimeter of transducer surface. Two different forming wires were tested. The first wire, a 4.5 mil 150 mesh metal wire, was chosen to minimize the wire impedance and investigate acoustic interaction with the fiber mat. The second wire, an 18 mil 80 mesh synthetic wire, was chosen to more closely model a commercial forming wire.

A refluidization parameter,  $\alpha$ , was developed based on analysis of each frame of the high speed digital video. After each test the camera contained 1365 frames of 512 by 384 pixel 8 bit grayscale image data showing the test cell, fiber mat and surrounding area. Each

frame in turn was cropped to show only those pixels inside of the test cell. The frame was then binarized and a pixel count established the ratio between the image space occupied by fibers and that occupied by fluid. The refluidization parameter was then defined such that it was equal to zero, when this pixel ratio was equal to the ratio before the first impulse was triggered, and one if every pixel in the image was occupied by a fiber. This allowed a quantitative comparison between the relative ability of the different pulse durations and strengths to disrupt the fiber mat.

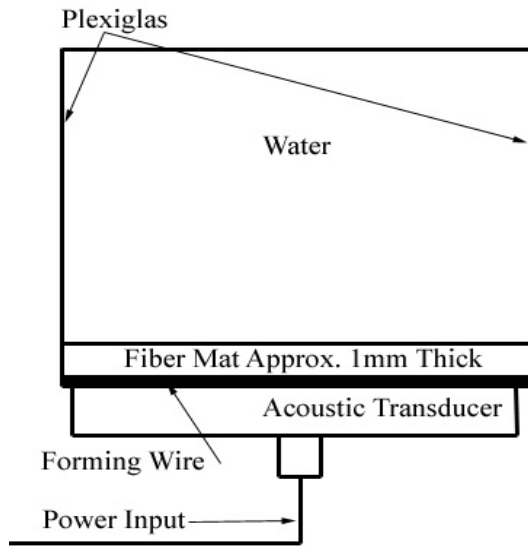
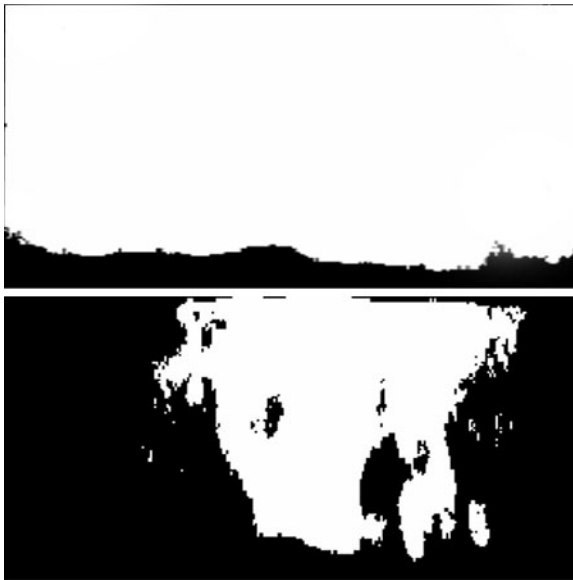


*Figure 2. Comparison between an undisturbed mat,  $\alpha = 0$ , at the top and a refluidized mat,  $\alpha = 0.5$ , on the bottom after four pulses.*

*Figure 1. Schematic of the test setup.*



#### IV. Results

The most extensive tests were conducted on the 150 mesh wire with each pulse duration tested at each power level. It was shown that holding power constant at 8 Watts/cm<sup>2</sup> a pulse duration of 60 ms or longer was sufficient to substantially refluidize the mat after four impulses. No additional refluidization was realized by longer pulses. A pulse duration of 30 ms served to somewhat refluidize the mat but the effect was much less than the 60 ms pulse. Holding the pulse duration constant at 60 ms, a power of 8 Watts/cm<sup>2</sup> or greater was sufficient to substantially refluidize the mat with no noticeable refluidization at 2 Watts/cm<sup>2</sup> and only minor effects at 4 or 6 Watts/cm<sup>2</sup>.

With the second wire we considered the effect of wire impedance and the consequent reduction in acoustic energy reaching the fiber mat. The increased impedance was enough to prevent refluidization at all but the highest power levels and longest impulse times with a greater than 50% reduction in refluidization even at these levels.

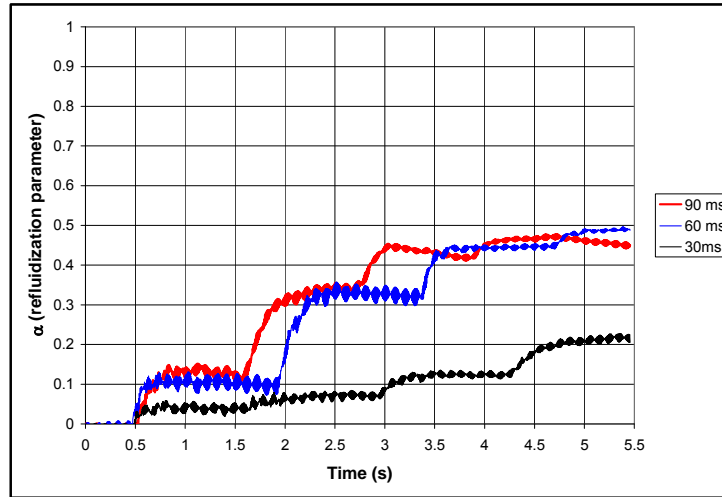


Figure 3. Refluidization on the metal wire at 8 Watts/cm<sup>2</sup> varying pulse duration.

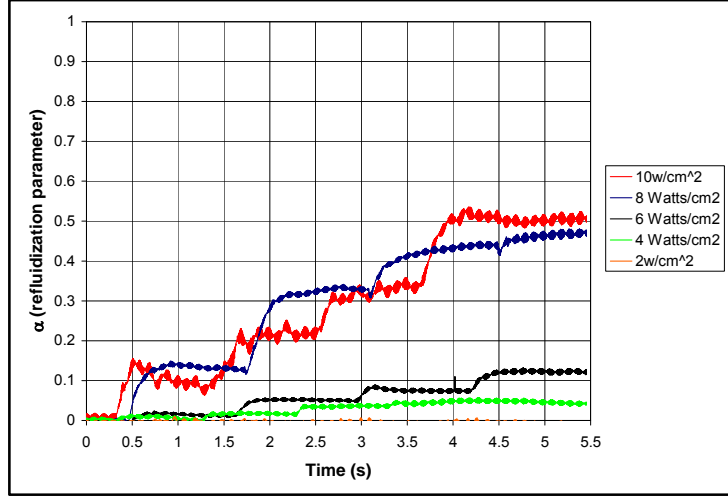


Figure 4. Refluidization on the metal wire with a 60 ms pulse duration varying power.

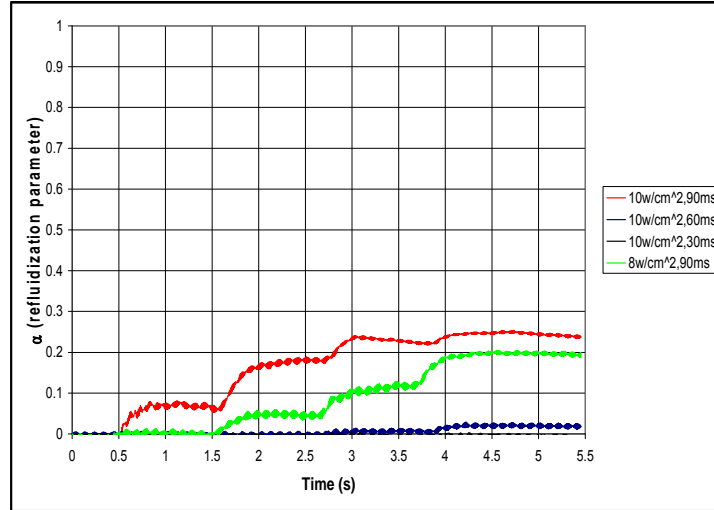


Figure 5. Refluidization on the 80 mesh wire at varying power and impulse durations.

## V. Conclusions

It has been shown that pulsed 150 kHz ultrasound has the ability to significantly disrupt and refluidize a wood fiber mat in water with pulse durations of 60 ms or greater and power input levels of 8 Watts/cm<sup>2</sup> or greater. The imposition of a wire with characteristics of a commercial forming wire between the transducer and fiber mat causes an impedance mismatch which significantly attenuates the refluidization but does not completely prevent it at high power levels and long pulse durations. Further work to match the transducer impedance to the forming wire and to increase the efficiency of converting electrical power to acoustic power should greatly enhance the ability to disrupt mats through realistic forming wires and at pulse durations comparable to the residence time of a fiber over the transducer head on a high speed forming section.

## VI. References

1. Sondegren, O. F. and J. A. Neun, 'Developments in Activity Generation on Fourdriners', TAPPI Journal, Vol 83 (10), 2000
2. Datar, G. V., P. Banks-Lee and P. L. Grady, 'Acoustical Properties of Fabrics in Low-Intensity Ultrasound', Applied Acoustics, Vol 47, 345-350, 1996
3. Datar, G. V., P. Banks-Lee and P. L. Grady, 'Acoustical Properties of Fabrics in High-Intensity Ultrasound', Applied Acoustics, Vol 48, 33-45, 1996
4. Shoshani, Y. and G. Rosenhouse, 'Noise Absorption by Woven Fabrics', Applied Acoustics, Vol 30, 321-333, 1990
5. Brodeur, P. 'Motion of Fluid-Suspended Fibres in a Standing Wave Field', Ultrasonic, Vol 29, 302-307, 1991

## QUANTIFIED BENEFITS TO THE INDUSTRY SHOULD THE TECHNOLOGY BE COMMERCIALIZED

The economic benefits of the acoustic dewatering technology are machine and grade dependent. The estimated savings with this technology are based on 10% improvement in formation, 10% reduction in MD/CD tensile ratio, and 5% improvement in rate of drainage. The IPST economic model contracted from Jaakko Pöyry is used by Dr. David White, Assistant VP of Technology Transfer at IPST.

It is estimated that the drainage on the wire can be increased by 5% or more with the addition of an acoustic foil. The increase in drainage results in increased productivity and lower cost. Also, formation can be improved by 10% or more and the MD/CD ratio in tensile can be decreased by about 10%. Formation improvement results in enhanced quality in printing and other converting processes, as well as increase in strength properties, such as burst, with consequent reduction in basis weight. This would yield fiber savings (per unit area of product), a commensurate reduction in drying energy, and some further energy savings due to reduced over-drying of lighter weight areas in the sheet. The savings in fiber cost are estimated at \$5.4 million Dollars per year (\$3.4 MM in fiber savings and \$2 MM in energy savings) for a 1000 ton/day machine. The benefits of 5% increase in drainage, based on use of the IPST Economic Model, results in increase in operating profit (revenues – costs – depreciation) of 12 million Dollars per year or \$34/FMT. The annual cost of the electric power to operate the acoustic foil is estimated at \$10,880 ( $= .0035 \text{ KW/cm}^2 * 20 \times 600 \text{ cm}^2 * 24 \text{ Hx360D} * \$0.03 \text{ per KWH}$ ). The cost of an acoustic foil is estimated at \$250K per element; a small capital investment with an ROI of 2 to 3 months.

## APPENDIX

### **1. Introduction**

We have had considerable progress in this project characterizing the acoustic transmission and interaction with a forming wire and investigation of the ‘ringing’ effect near the surface of the wire. We have estimated the ‘region of influence’ of the acoustic interaction with the wire to range from 3 mm with the 4 MHz transducer to about 6 mm with the other transducers. More details are provided below. This study has been part of the Paper Science and Engineering MS thesis by Lyle Fouts and Matthias Messer.

### **2. Ultrasonic Field Measurement Setup:**

The pulsed Doppler ultrasound velocimetry instrument DOP2000 model 2125 by Signal Processing was used to measure the ultrasonic field generated by various ultrasonic transducers. The transducers used with this system are both transmitters and receivers. The effect of paper forming screens placed between the ultrasonic transducer and the area of interest (an object reflecting the ultrasonic wave packet emitted by the transducer – in this case: plastic sphere) was evaluated. The sphere was used in order to reflect a source of ultrasonic energy from a single point to the transducer. The ultrasonic transducer and plastic sphere were submerged in water as shown in Figure 0-1. The plastic sphere and the ultrasonic transducer were mounted on xyz-positioners as shown in Figure 0-2. It should be remembered that the beam characteristics measured in water are different from those in water with suspended fibers or particles. Nevertheless, a great deal can be deduced about a beam in water with suspended fibers or particles from a plot obtained in water.



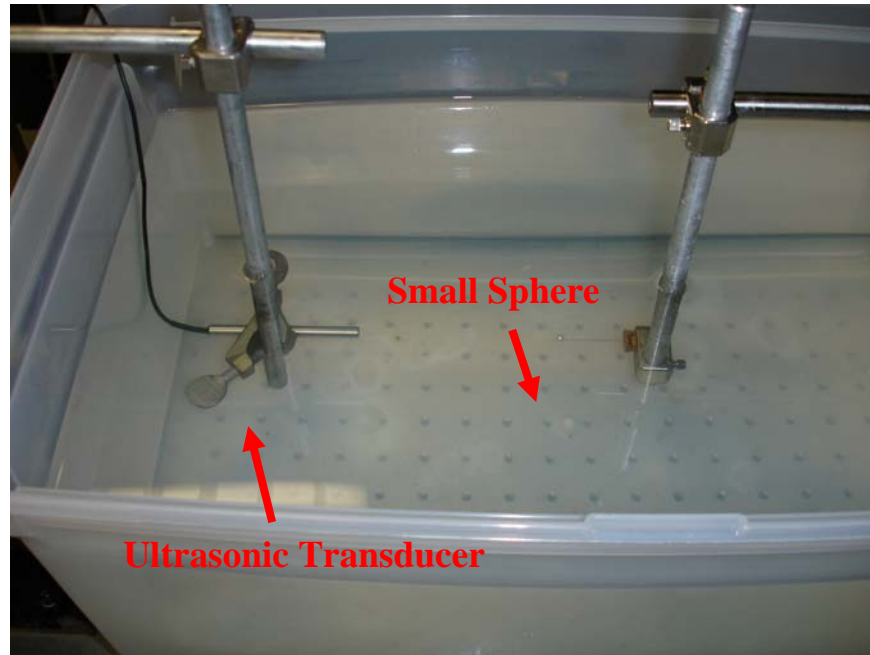


Figure 0-1: Experimental Setup

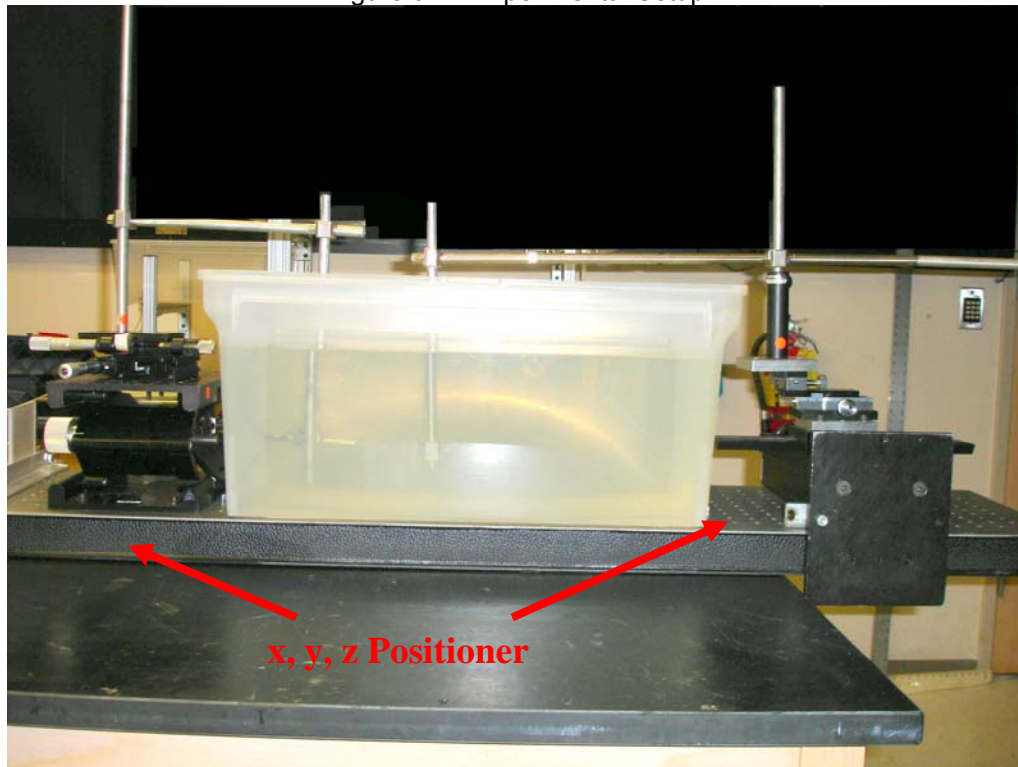


Figure 0-2: Experimental Setup with x, y, and z Positioning

Figure 0-3 shows the basic experimental setup used to measure the ultrasonic field. The distance between the sphere and the surface of the transducer on the x-axis is defined as  $\Delta x$ . The ultrasonic signal propagates along the x-axis; therefore, the ultrasonic beam is

symmetric about the x-axis. Y and z are the movements perpendicular to the x-axis, or ultrasonic beam axis.

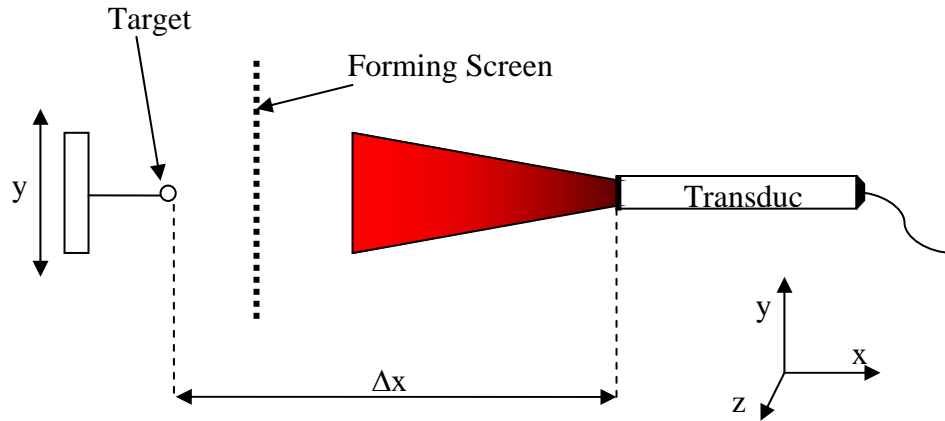


Figure 0-3: Schematic of Beam Measurement test setup

The sphere was attached to a small rigid rod (maximum 1/3 of the diameter of the sphere). The length of the rod was 3 cm. The system, rod, and sphere, are mounted on a xy-table which is capable of positioning the sphere with a minimum resolution of 0.1 mm (Figure 0-2). The system, sphere, and transducer, are completely submerged. Since the maximum distance between the transducer and the plastic sphere in the following tests will be 120 mm, the transducer and plastic sphere were submerged approximately 150 mm below the surface of the liquid. This ensured that the transducer and sphere were surrounded by enough liquid in order to avoid the influence of the free surface of the liquid. If the free surface of the liquid was closer to the transducer or sphere than 120 mm, the liquid surface could cause a false echo, or artifact, in the ultrasonic beam shape experiments.

The measurement of the ultrasonic field generated by an ultrasonic transducer was realized by measuring the intensity of an echo coming from the plastic sphere. By moving the position of the sphere along a line perpendicularly (y-axis) to the axis of the ultrasonic beam (x-axis) the intensity of the echo for different positions of the sphere were measured (it is assumed that the z-axis is symmetric about the y-axis). This data was used to analyze the -3dB and -6dB width of the ultrasonic beam. Figure 0-3 illustrates the principles and experimental setup for the method. After selecting various control parameters, centering and placing the sphere at the desired depth, the ultrasonic field can be measured.

At first, ultrasonic beam measurements of four different transducers were conducted. Then a paper forming screen was placed between the transducer and the plastic sphere (area of interest) as shown in Figure 0-4 and Figure 0-5.

Ultrasonic beam measurements of the following transducers were conducted:

- Transducer 1: 2 MHz emitting frequency, 10 mm transducer diameter
- Transducer 2: 4 MHz emitting frequency, 5 mm transducer diameter
- Transducer 3: 8 MHz emitting frequency, 5 mm transducer diameter
- Transducer 4: 4 MHz emitting frequency, 8 mm transducer diameter, focused

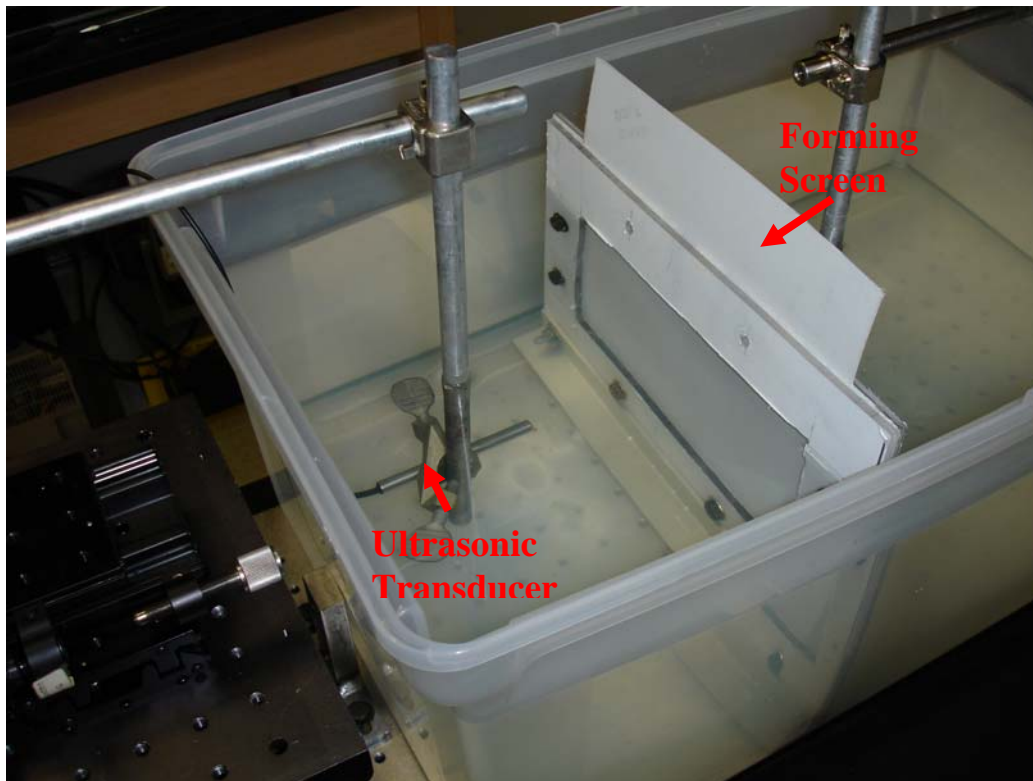


Figure 0-4: Beam Shape Measurement Setup with Forming Screen

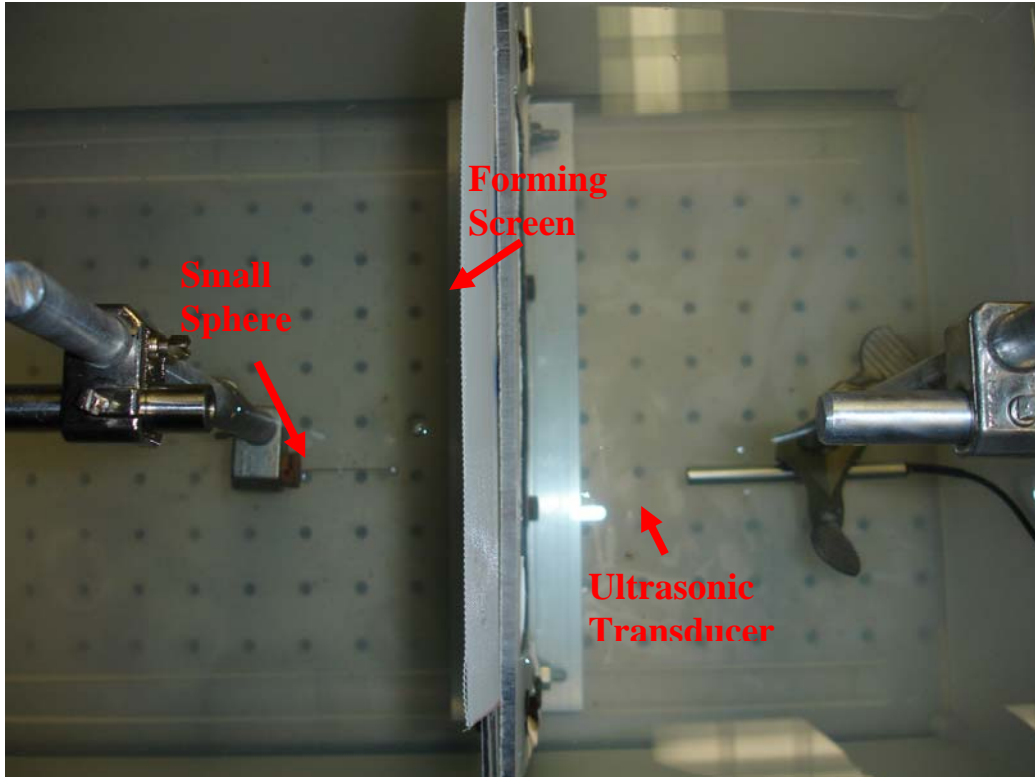


Figure 0-5: Beam Shape Measurement Setup with Forming Screen (Plan View)

The amplitude of the received echo in volt as a function of the distance between the plastic sphere and the transducer center on the y-axis and the general beam divergence of each transducer are presented in the following section. In all echo amplitude plots, the distance between the plastic sphere and the transducer face on the x axis ( $\Delta x$ ) is plotted as a function of the distance between the plastic sphere and the transducer center on the y-axis.

#### Ultrasonic Field Procedure:

The measurement of the ultrasonic field using the Signal-Processing DOP 2000 was performed using the following procedure as stated in the Signal-Processing handbook [31]:

1. *The test setup should be as described above (Figures 2-1 through 2-5) with an x,y,z-positioner for the transducer and for the target sphere.*
2. *Before entering in the menu dedicated to the measurement of the ultrasonic field, the following procedure must be executed in the supplied software:*
  - a. *recall default factory settings;*
  - b. *choose emitting frequency corresponding to transducer being used;*
  - c. *select a emitting power of "Low";*

- d. select a burst length of 4 cycles;
  - e. define overall TGC of 20 dB;
  - f. select a spatial filter of 1.05mm.
3. Enter the ultrasonic field measurement menu found in the "Advanced compute" tab.
  4. Place sphere in contact with transducer in order to find the center of the ultrasonic beam field in the y and z plane. The sphere should now be centered with the transducer on the x axis.
  5. Place the sphere at the desired depth,  $\Delta x$ , without moving the y and z directions of the sphere.
  6. Enter the depth,  $\Delta x$ , in the field labeled "at Z" ("Measure mm" panel) and in "Start at" ("parameters" panel). Also, select a PRF of 1500 and a number of gates equal to 200. The "Start at" depth can be a few mm lower than the actual depth of the desired measurement, but the closer the desired depth is to the horizontal axis on the echo modulus graph, the better the results that were obtained for this series of tests.
  7. The amplification (TGC and module scale) can now be adjusted in order to obtain a clear and strong echo from the sphere. Take care in identifying clearly the echo from the sphere and not from any of the objects holding the sphere. The amplitude should be set to the lowest number possible, but the peak of the echo modulus should ideally take up approximately 2/3-3/4 of the horizontal axis of the echo modulus graph.
  8. Once amplification is set, select the number of gates to be 40 (make sure the gates encompass the echo of the sphere on the echo modulus graph). Also make sure that any changes in the PRF value (up or down) do not induce changes in the shape or value of the echo from the sphere. If artifacts are present (something other than the sphere), find PRF values where no artifacts appear.
  9. Now you are ready to measure a slice. Define the maximum y distance from the transducer axis from which you will start the measurement and step between the points. Enter these values in their corresponding field in the panel "Measure mm". Be sure that the depth  $\Delta x$  at which the measurement will be realized is also displayed in the corresponding field. Then:

- a. Click on the button labeled “Add new slice”. A new button labeled “Measure” will appear, and just below this button the y-axis value at which you must place the sphere. Move the sphere to that position.
- b. Click on the button “Measure” or press the space bar to record the first point of the slice.
- c. Move the sphere a step forward and wait a little bit in order to let the system stabilize. Then press again on the space bar to record a new point.

A slice is simply a set of amplitude data points from a certain depth,  $\Delta x$ . For the tests in question, a step size of 0.5 mm was used for a total span of 20 mm.

10. There is no limit to the number of slices that can be added, but each slice must have a unique depth. For each slice that is measured, repeat the steps from step 6 above.

## Ultrasonic Beam Field

Ultrasonic beam measurements are conducted to gain information about the actual beam shape of the given ultrasonic transducers and especially their lateral resolution. These ultrasonic beam measurements will then be used to analyze the effect of porous screens on various measurements. Before investigating the ultrasonic beam shape with porous screens between the transducer and the area of interest (plastic sphere), the beam shape of various transducers is determined with no screen present.

### 3. Echo Amplitude

At a certain distance (minimum distance) between the transducer and the plastic sphere on the x-axis, measurements of the ultrasonic beam shape become impossible due to the transducer's ringing effect. This ringing effect is characterized by a saturation of the transducer preventing measurements. This is indicated by the ultrasonic system showing a strong echo profile in a region of the test medium where there is no object present that could register an echo. When the ultrasonic transducer attempts to take measurements in a saturated region, the DOP 2000 system returns an amplitude value that is several orders of magnitude greater than the amplitude recorded in a region that is not saturated. The system also records a beam width of zero. Further decreasing the  $\Delta x$  beyond this minimum distance between the transducer and the plastic sphere on the ultrasonic beam axis (x-axis) does not yield any useful measurement results of the ultrasonic beam shape. This is due to the fact that the ultrasonic echo of the plastic sphere can not be recognized in between the high echo amplitudes caused by the transducer's ringing effect. Ringing effects following the emission of the ultrasonic wave packet cause a region of strong echoes (saturation) at depths located just after the surface of the transducer. In this region, the ultrasonic field can consequently not be measured. For this study, the region of high echo amplitudes caused by the transducer's ringing effect is called "saturation region". The distance between transducer and plastic sphere at which the saturation region begins is called the "minimum distance". Increasing the amplification in the instrument consequently increases the transducer's ringing effect; therefore, increasing the amplification increases the saturation region and the minimum distance. This means that the smallest possible amplification level that gives an accurate measurement should be used, especially for measurements that are close to the ultrasonic transducer.

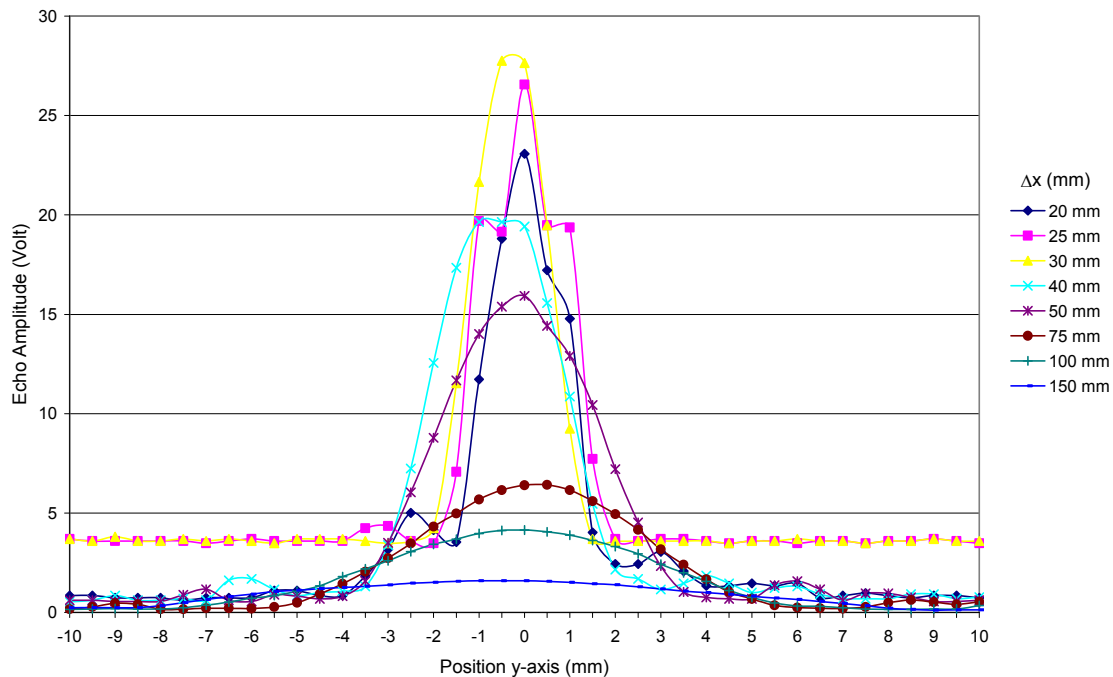


Figure 0-1: Echo Amplitude 2 MHz 10 mm Transducer

Figure 0-1 shows a plot of the amplitude of the 2 MHz 10mm transducer as a function of the position of the plastic sphere. The echo amplitude forms a maximum located on the ultrasonic beam axis (x-axis). As soon as  $\Delta x$  becomes smaller than the minimum distance the overall echo amplitude level increases. Further decreasing  $\Delta x$  leads to a straight line at relatively high echo amplitudes. In this case, the echo of the plastic sphere can not be recognized in between this “saturation region.” Therefore, at a certain minimum distance, beam shape measurements become impossible. The DOP 2000 device simply records a value of zero for the width of the beam.

Using a 2 MHz ultrasonic transducer, the saturation region is ideally 10 – 15 mm wide. In the saturation region, no valid measurements are obtained, therefore, when using the 2 MHz ultrasonic transducer, the area of interest had to be at least 15 mm away from the ultrasonic transducer. As shown in Figure 0-1 the smallest  $\Delta x$  measurement recorded was 20 mm due to the fact that the amplitude was larger on the periphery of the beam measurement in comparison to the much smaller values of amplitude on the periphery of the beam measurements for the  $\Delta x$ 's that were 30 mm and greater. Further decreasing the  $\Delta x$  for this



transducer would result in a much larger value for the amplitude with no change in the value for the entire span of the y-axis. A decrease in  $\Delta x$  would also produce a beam width measurement of zero.

Using a 4 MHz transducer, the region of strong echoes is ideally 3 – 8 mm, depending on the chosen amplification. In this test set-up, the minimum distance is 5 mm for the unfocused 4 MHz (Figure 0-2) and 4 mm for the focused 4 MHz ultrasonic transducer (Figure 0-3), respectively. For the 8 MHz transducer, values of ideally 3 – 5 mm can be obtained, but the minimum distance for the 8 MHz transducer is 8 mm as shown in Figure 0-4. In general, the minimum distance decreases with increasing frequency. Since much stronger attenuation occurs to the ultrasonic signal emitted by the 8 MHz transducer than the ultrasonic signal emitted by the 4 MHz transducer, a higher amplification must be used when working with the 8 MHz transducer. This caused the minimum distance of the 8 MHz transducer to increase and is therefore higher than the minimum distance for the 4 MHz transducer. The amplitude plots show maximum amplitudes of 73 and 325 volt for the 4 MHz and 4 MHz focused transducers, respectively. This shows that the focused transducer receives more energy in its echo from the small sphere than the unfocused transducer. This is due to the fact that the ultrasonic energy emitted from the focused transducer is focused, or more concentrated itself, therefore, more of the ultrasonic energy is reflected back to the transducer by the small sphere causing a much higher amplitude measurement.

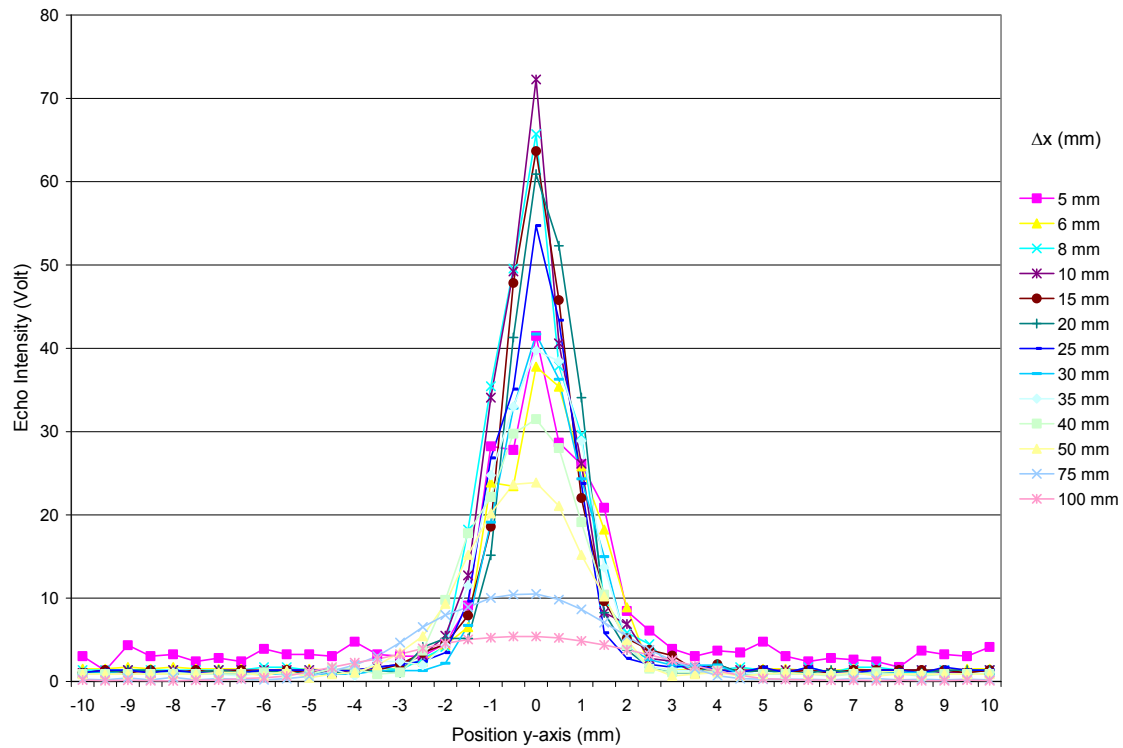


Figure 0-2: Echo Amplitude 4 MHz 5 mm Transducer

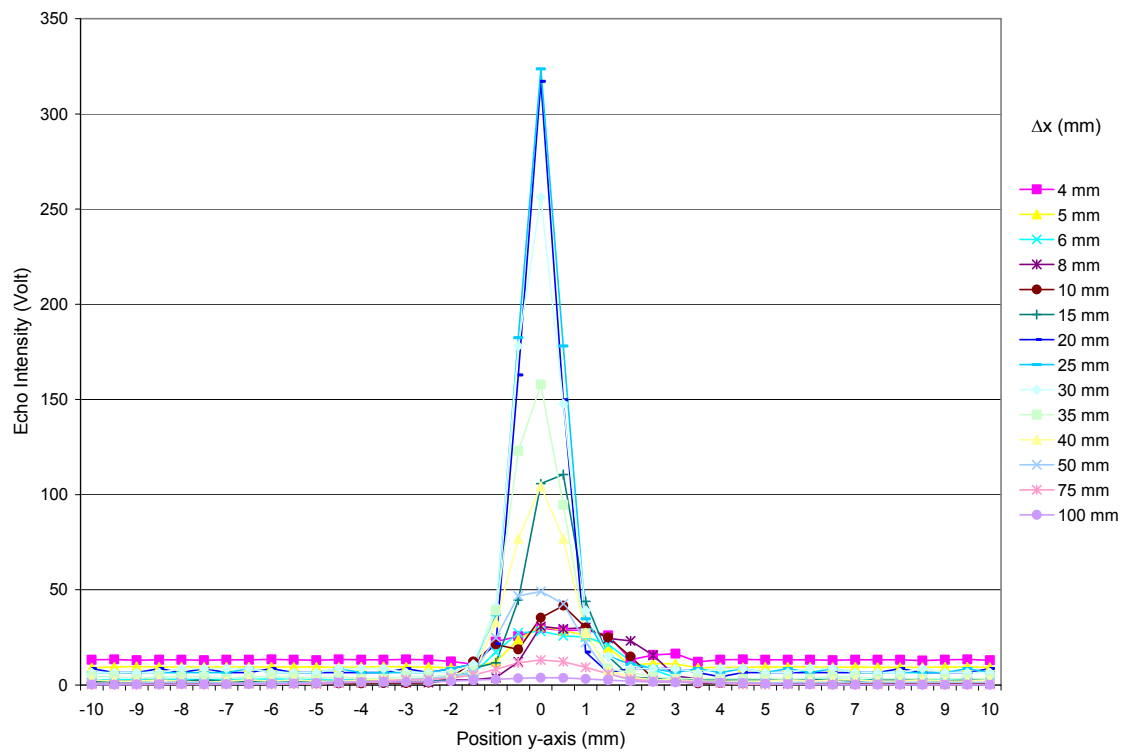


Figure 0-3: Echo Amplitude 4 MHz 8 mm Focussed Transducer

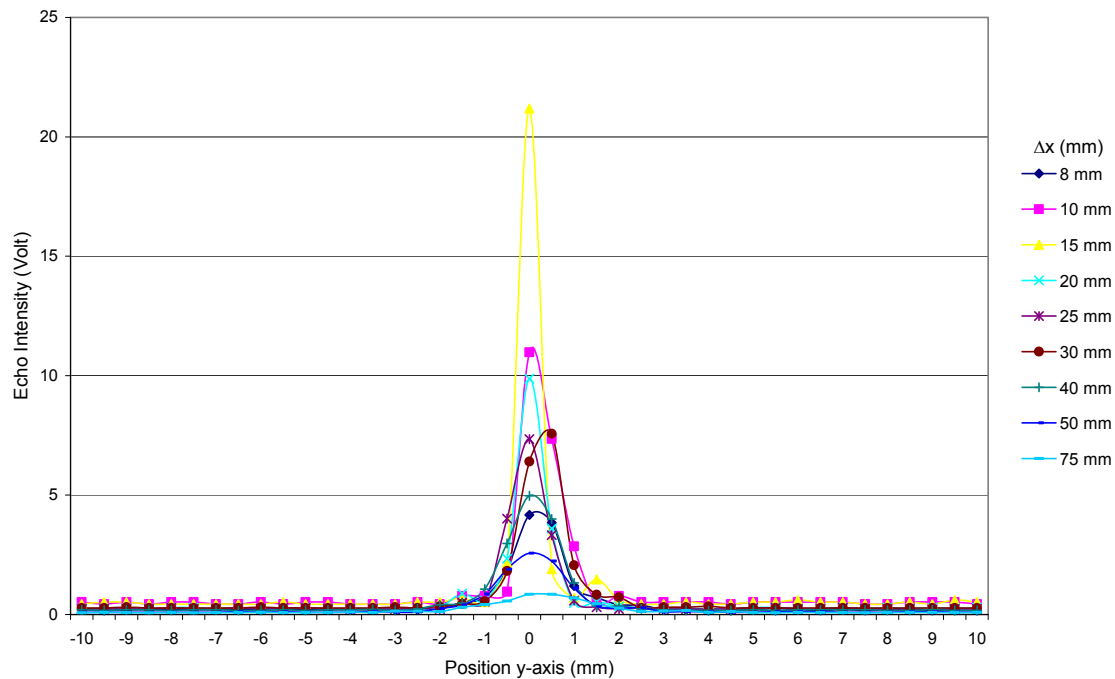


Figure 0-4: Echo Amplitude 8 MHz 5 mm Transducer

### Ultrasonic Beam Shape

Ideally, the ultrasonic beam emitted from the transmitter should be a conic in shape. With no obstructions present in the ultrasonic field, Figures 3-5 through 3-8 show that the ultrasonic beam is, in fact, conic in shape. These figures also show that the beam width in the far field decreases with increasing transducer size (greater aperture). In the same way as beam width, beam divergence decreases with increasing frequency. The half angle of beam divergence (given by the instrument) for the 2 MHz 10 mm transducer is 2.27 degrees, 2.23 degrees for the 4 MHz 5 mm transducer, 1.22 degrees for the 8 MHz 5 mm transducer and 2.33 degrees for the 4 MHz 8 mm focused transducer. This is shown in Table 3-1. Theoretically beam divergence in the far field should be less for larger than smaller diameter transducers [12]. This shows that the half angle of beam divergence is smaller for the unfocused 4 MHz 5 mm than for the focused 4 MHz 8 mm transducer. Consequently, when comparing focused and unfocused ultrasonic transducers the claim that beam divergence in the far field should be less for larger diameter than smaller transducers is not justified. Unfortunately unfocused ultrasonic probes of the same frequency with different diameters

were not available to experimentally validate this theoretical claim. Theoretically, for a given transducer frequency the near field length should also be greater for larger diameter transducers, and for a given transducer diameter the near field length should theoretically be greater for higher-frequency transducers [12].

The ultrasonic beam divergence profile of the 2 MHz transducer (Figure 0-5) shows that this transducer is not suitable for measuring velocity profiles in small channels or where measurements are made close to the transducer due to the relatively large minimal measurable distance of 20 mm and the poor lateral resolution. The 2 MHz transducer could be placed at a distance of 20 mm away from the region of interest, but acoustic coupling and anomalies such as wall effects decrease the quality of achieved measurement results. The 4 and 8 MHz transducers (Figure 0-6, Figure 0-7, and Figure 0-8) are best suited for measuring velocity profiles when dealing with small geometries. Due to the better lateral and axial resolution (smaller beam diameter and short ultrasonic pulse length) of the unfocused 8 MHz transducer, compared to the unfocused 4 MHz transducer, the unfocused 8 MHz transducer is theoretically best suited measurements in small geometries described above (in actuality, when conducting experiments involving forming screens, the unfocused 4 MHz transducer produced the best results as presented in a later section).

Table 0-1: Half-Angle Beam Divergence of Various Transducers

Transducer	Half-Angle Beam Divergence
2 MHz 10 mm	2.27°
4 MHz 5 mm	2.23°
4 MHz 8 mm Focused	2.33°
8 MHz 5 mm	1.22°

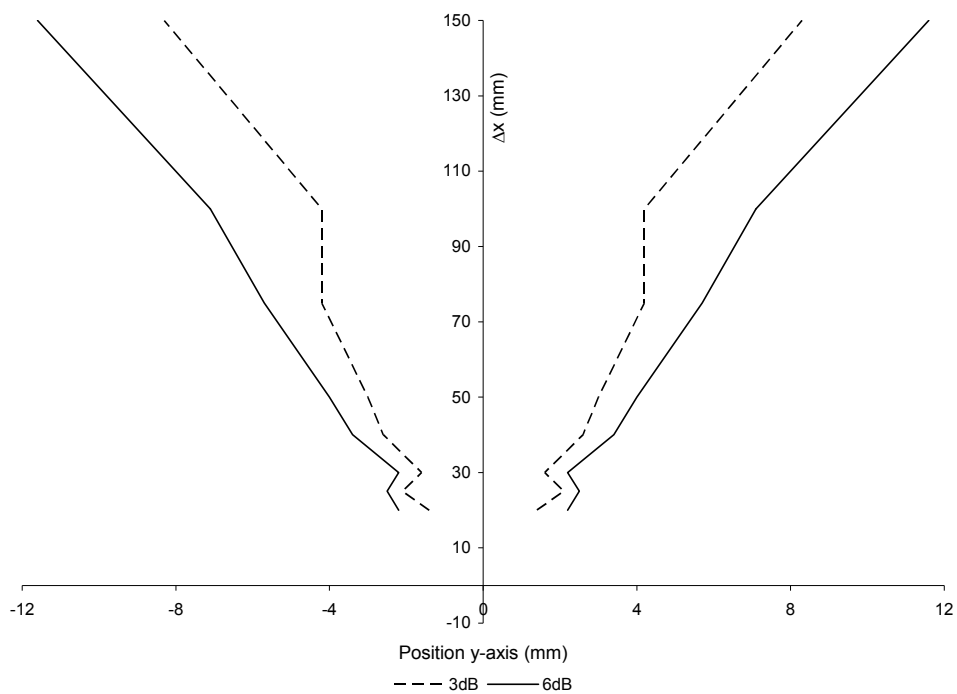


Figure 0-5: Beam Divergence Profile for 2 MHz 10 mm Transducer

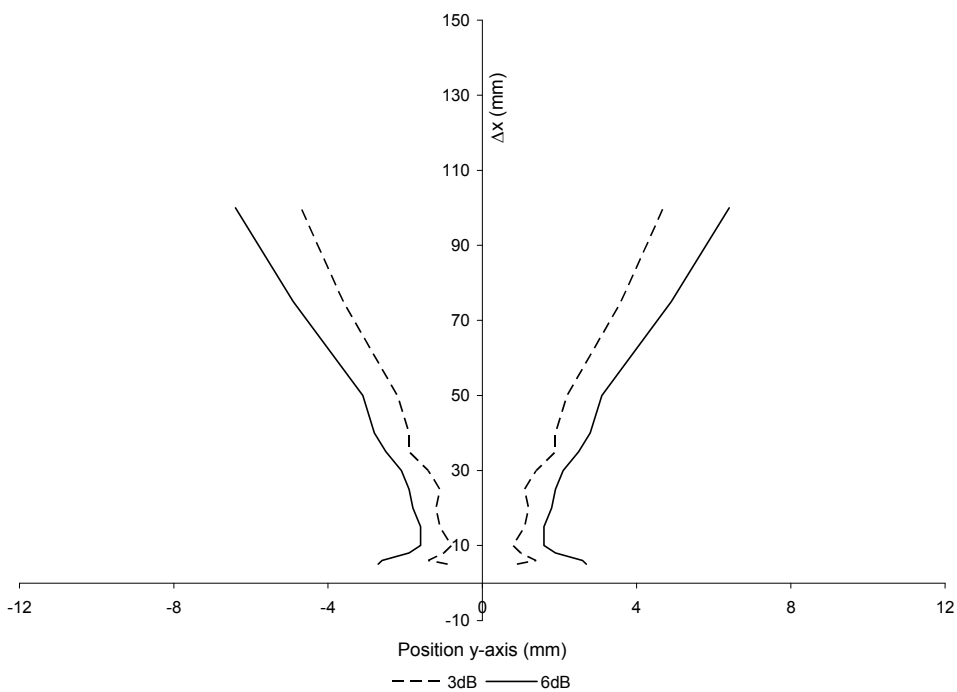


Figure 0-6: Beam Divergence Profile for 4 MHz 5 mm Transducer

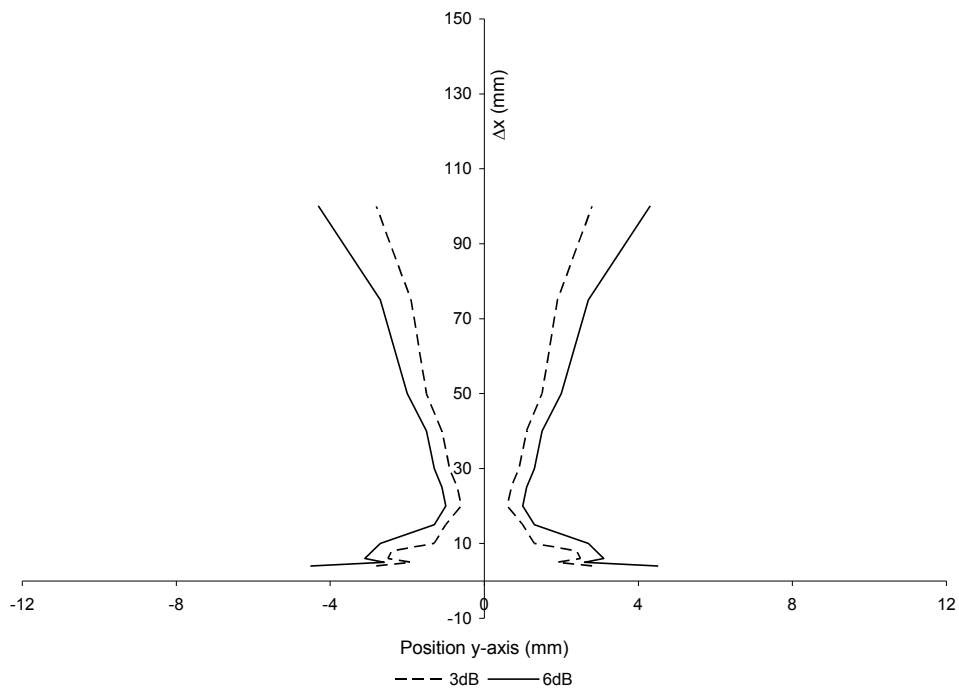


Figure 0-7: Beam Divergence Profile for 4 MHz 8 mm Focused Transducer

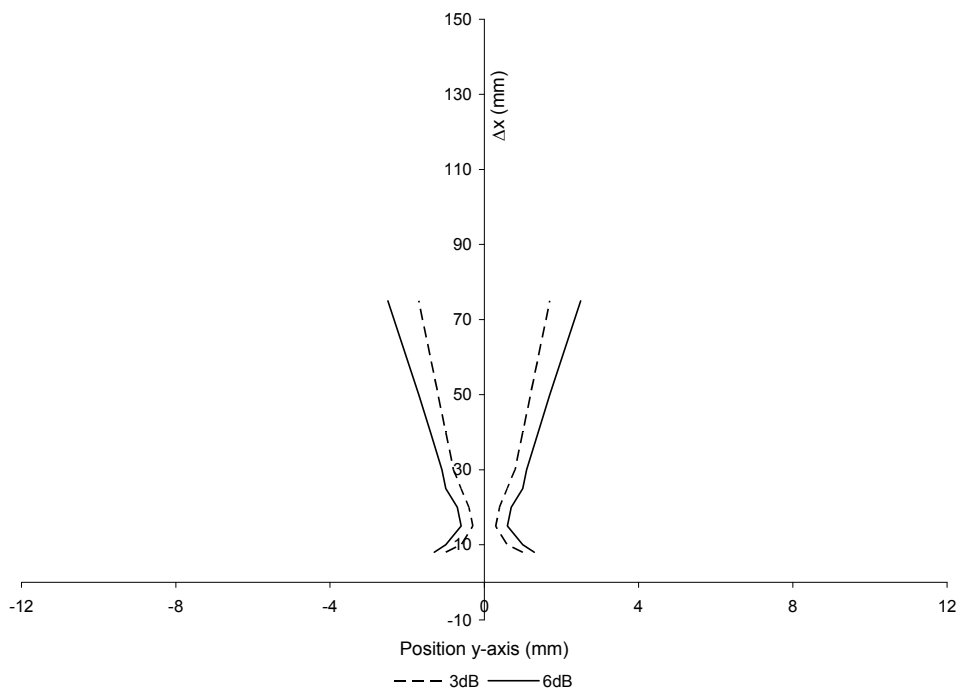


Figure 0-8: Beam Divergence Profile for 8 MHz 5 mm Transducer

A comparison of the beam divergence profiles for the 4 MHz 5 mm and the 8 MHz 5 mm transducers is shown in Figure 0-9. This figure shows that at a given transducer diameter, the beam width decreases with decreasing wavelength because wavelength is inversely proportional to frequency. Beam width consequently decreases with increasing frequency. The fact that for a large ratio of diameter to piezoelectric element thickness the ultrasonic beam is focused can clearly be seen in Figure 0-9. The 4 and 8 MHz transducer both have a transducer diameter of 5 mm. Since the thickness of the piezoelectric element equals half of the desired wavelength, the ratio of the diameter to the piezoelectric element thickness for the 8 MHz 5 mm transducer is larger than for the 4 MHz 5 mm transducer. Therefore, the unfocused 8 MHz 5 mm ultrasonic transducer is focused in contrast to the unfocused 4 MHz transducer.

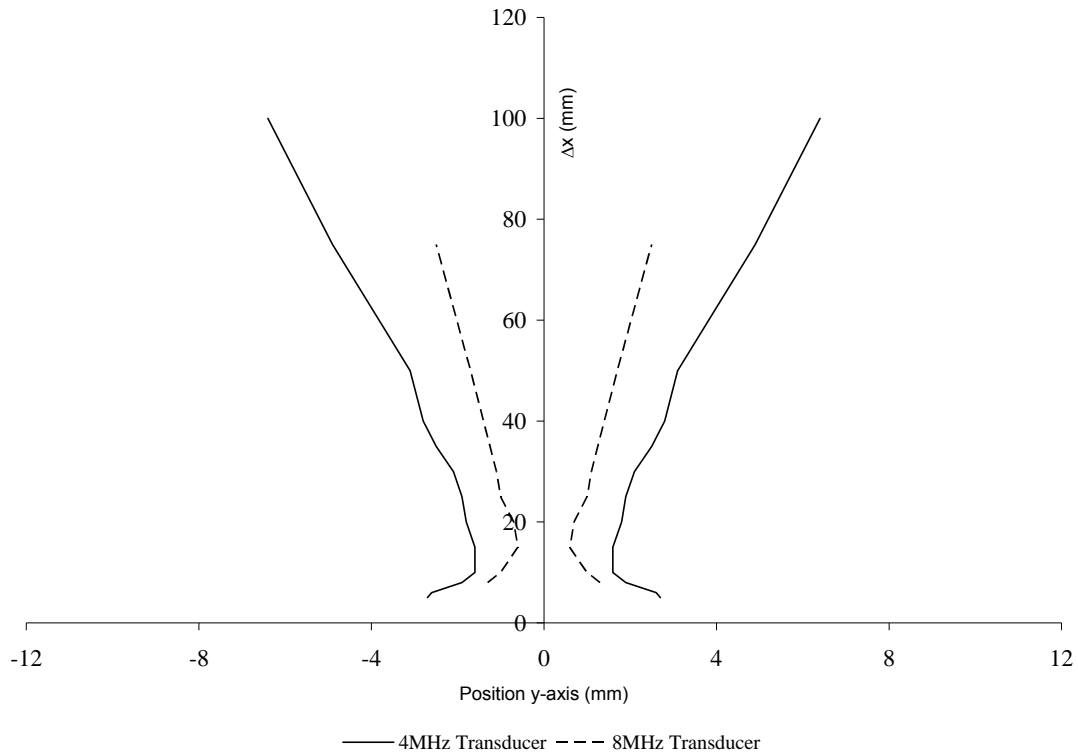


Figure 0-9: Beam Divergence Profiles for the 4 MHz 5 mm and 8 MHz 5 mm Transducers

The focused 4 MHz 8 mm transducer was also compared to the unfocused 4 MHz 5 mm transducer in order to compare measurement results of unfocused and focused ultrasonic transducers. The focal point of the focused 4 MHz 8 mm transducer is approximately 20 mm

away from transducer face ( $\Delta x$  of 20 mm). The beam width of the focused transducer is approximately half of the beam width of the unfocused transducer at the focal point as shown in Figure 0-10. Due to focusing the ultrasonic beam and consequently the ultrasonic energy, the amplitude of the received echo from the 4 MHz focused transducer is increased by approximately 500 percent at the focal point and approximately 20 percent at the focal point of the unfocused 8 MHz 5 mm transducer (see Figure 0-2 through Figure 0-4) when compared to the amplitude of the received echo of the 4 MHz unfocused transducer. The focal point of the ultrasonic beam of the unfocused 8 MHz 5 mm transducer (due to the large ratio of diameter to piezoelectric element thickness) is at a  $\Delta x$  of approximately 15 mm. The echo amplitude is of the same order of magnitude before and after the focal point for the focused and unfocused transducer. The minimal distance at which measurements are possible is of the same order for the focused and unfocused transducer. It can clearly be seen that the beam width in the far field is smaller with the focused transducer (Figure 0-10). This is also due to the larger aperture of the focused transducer.

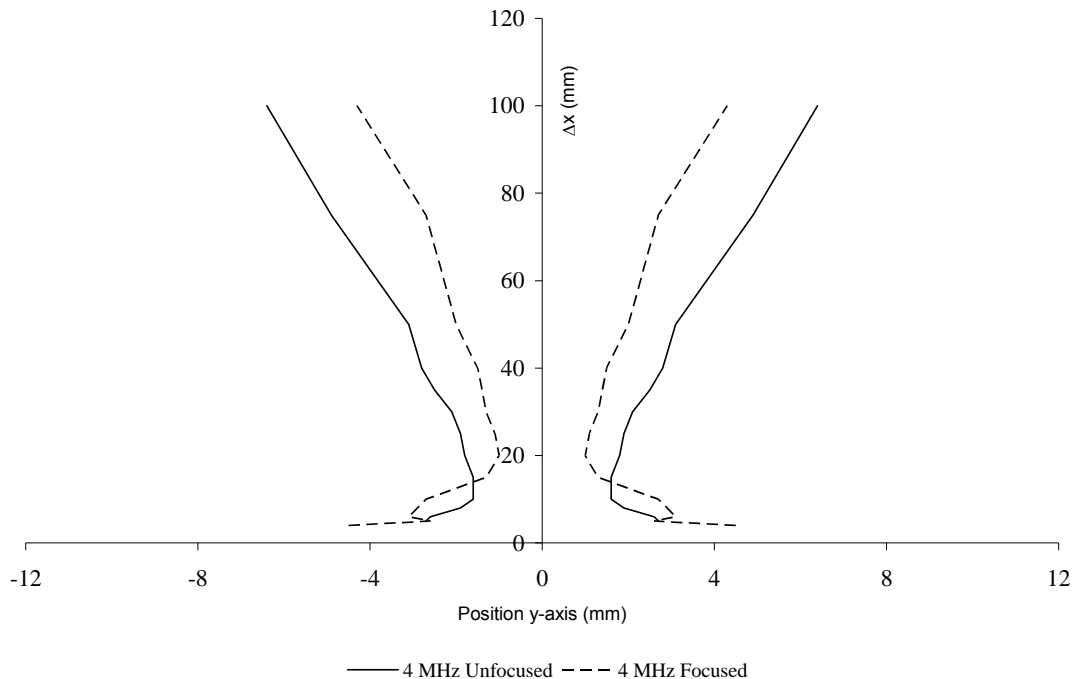


Figure 0-10: Beam Divergence Profiles for the 4 MHz 5 mm and 4 MHz 8 mm Focused Transducers

In industrial applications measurements of the velocity profile in the area close to forming screens is most important. Therefore, the distance from the screen to the



plastic sphere at which the echo of the plastic sphere can still be recognized must be as small as possible. A forming screen is placed at various distances on the x-axis in order to find the smallest measurable plastic sphere-screen distance. In evaluating the measurement results of the forming screen, emphasis is placed on finding the closest distance from the plastic sphere to the screen over the widest range of transducer-screen-distances ( $\Delta x$ ) that produces detectable echoes of the plastic sphere behind the forming screen.

#### 4. Forming Screen Specifications

Two different forming screens were used in this study, forming screen A (ScreenA) and forming screen B (ScreenB). A microtomographic view of ScreenA is shown in Figure 0-11. ScreenA has the following properties:

- Material: Polyester
- Density Polyester:  $1.35 \text{ g/cm}^3 = 1350 \text{ kg/m}^3$
- Fiber volume:  $0.38 \text{ cm}^3$
- Pore volume:  $0.36 \text{ cm}^3$
- Porosity: 0.95
- Sample weight (in air): 0.57 g
- Sample weight (in water): 0.873
- Sample volume:  $0.74 \text{ cm}^3$
- Apparent density (in air):  $0.77 \text{ g/cm}^3 = 770 \text{ kg/m}^3$
- Apparent density (in water):  $1.18 \text{ g/cm}^3 = 1180 \text{ kg/m}^3$
- Thickness t:  $0.022 \text{ in} = 0.00056 \text{ m}$
- Mesh: 60 wires/inch = 2362 wires/meter
- Pore shape factor: 1 (cylindrical pores  $\approx$  cubical pores)
- Double layer:
  - i. Fiber diameter ply 1: 0.2 mm
  - ii. Fiber diameter ply 2: 0.4 mm
- Specific flow resistance: 95.5 MKS Rayls
- Sound Speed (Brodeur 1993): 1700 m/s

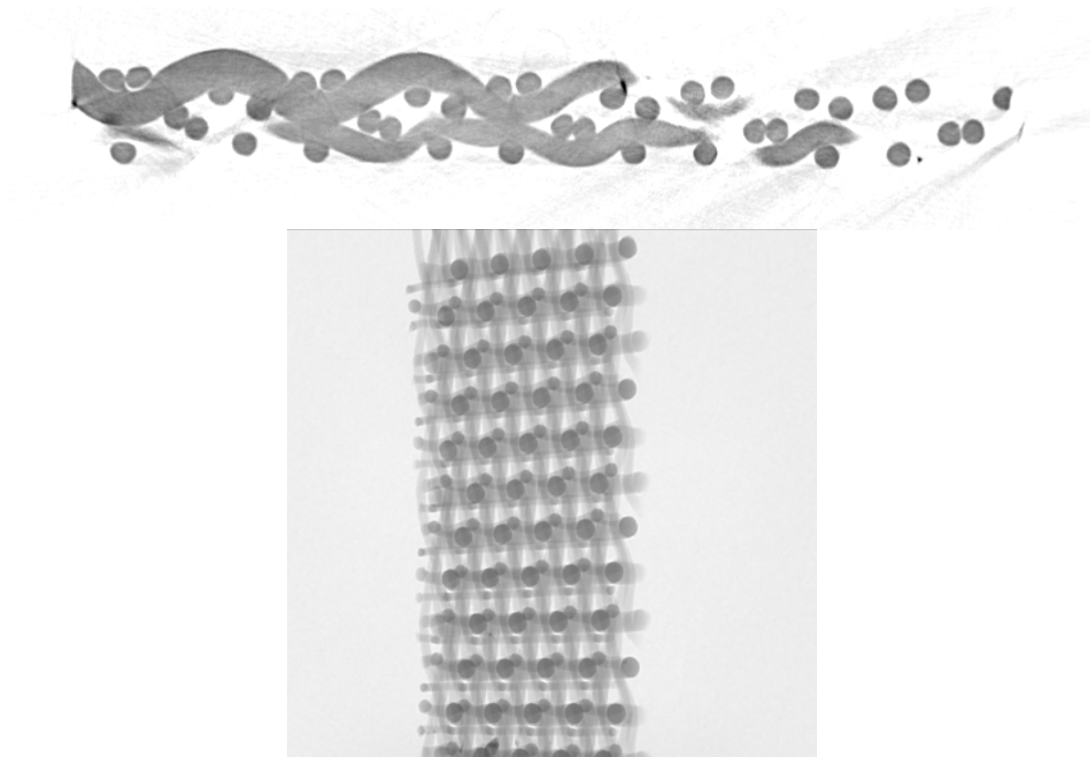


Figure 0-11: Microtomographic Cross-Section View Forming Screen

Forming screen B (ScreenB) was supplied by Albany International. It is fabric number F17263. ScreenB has the following properties:

- Material: Polyester
- Density Polyester:  $1.35 \text{ g/cm}^3 = 1350 \text{ kg/m}^3$
- Thickness t:  $0.054 \text{ in} = 0.00137 \text{ m}$
- Mesh:  $94 \text{ wires/inch} = 3700 \text{ wires/meter}$
- Count:  $89 \text{ wires/inch} = 3503 \text{ wires/meter}$
- Permeability:  $493 \text{ CFM} = 232 \text{ liters/second}$
- Pore shape factor: 1 (cylindrical pores  $\approx$  cubical pores)
- Design: CD125
- Style: TL
- Sound Speed:  $1700 \text{ m/s}$ .

Table 0-2: Comparison of Transducer Wavelength and Pore Size

Transducer	Wavelength ( $\mu\text{m}$ )	Screen Pore Size ( $\mu\text{m}$ )
------------	------------------------------	------------------------------------

2 MHz 10 mm	750	20 (ScreenA)
4 MHz 5 mm	375	70 (ScreenB)
8 MHz 5 mm	187.5	

### **Echo Amplitude and Beam Shape Measurements**

Placing a forming screen between the plastic sphere and transducer forces the echo amplitude to decrease due to the absorption and reflection of acoustic energy by the forming screen. When placing a forming screen between the transducer and plastic sphere, the foremost effect seen is a sharp decrease in the amplitude of the echo. A high amplification must be used to clearly recognize the echo coming from the plastic sphere behind the forming screen. For the 2 MHz 10 mm transducer, the decrease in the amplitude of the echo is 60 percent when ScreenA is between the plastic sphere and the transducer. When no screen is present, the maximum amplitude received by the transducer is 28 Volts (Figure 0-1), and when ScreenA is present (20 or 40 mm away from the transducer), the amplitude received by the transducer is 11 Volts. The amplitude plot for the 2 MHz 10 mm transducer when ScreenA is 40 mm away from the transducer is shown in Figure 0-12. This figure shows that the maximum amplitude received by the transducer when ScreenA was present was 11 Volts. For the 4 MHz 5 mm transducer, the decrease in echo amplitude is 93 and 96 percent for ScreenA and ScreenB, respectively, and with the 4MHz 8mm focused transducer, the decrease in the amplitude of the echo is approximately 94 percent. The maximum amplitude recorded by the 4 MHz 5 mm ultrasonic transducer was 75 Volts when no screen was present (Figure 0-2), 5.5 Volts when ScreenA was present (60 mm away from transducer) as shown in Figure 0-13, and 3 Volts when ScreenB was present (20 mm away from transducer) as shown in Figure 0-14. It should be noted that although there appears to be another maximum value in Figure 0-14 for the transducer measurements at  $\Delta x = 23$  mm, the measurements taken at  $\Delta x = 23$  mm were in the region saturated by ScreenB that causes the ringing effect. This means that this slice, or set of measurements, does not give meaningful results. The maximum amplitude recorded by the 4 MHz 8 mm focused ultrasonic transducer with

the forming screen absent was 325 Volts (Figure 0-3), and the maximum amplitude that was recorded by the ultrasonic transducer when ScreenA was present was 21 Volts when the forming screen was 20 mm away from the transducer as shown in Figure 0-15. The 8 MHz 5 mm transducer had a decrease of 100 percent in echo amplitude. No results were achieved for the 8 MHz transducer when ScreenA was in place due to the high absorption rate. In all cases, the reduction in amplitude when the forming screen was present was very significant. These trends show that the echo amplitude decreases with increasing frequency since attenuation of acoustic waves increases with increasing frequency. This trend of decreasing echo amplitude with increasing frequency is the reason that the 8 MHz 5 mm transducer did not yield useful results. It simply did not have enough acoustic energy to create a detectable echo. The echo amplitude decreases with increasing distance between the transducer and the screen. All cases show a significant decrease in echo amplitude for the case when the forming screen is between the plastic sphere and transducer. Table 0-3 shows a summary of the maximum echo amplitudes recorded with and without the forming screens present.

Table 0-3: Summary of Echo Amplitudes

<b>Screen A</b>			
Transducer	Maximum Amplitude without Screen Present	Maximum Amplitude with Screen Present	Percent Decrease in Amplitude
2 MHz 10 mm	28 Volts	11 Volts	60%
4 MHz 5 mm	75 Volts	5.5 Volts	93%
4 MHz 8 mm Focused	325 Volts	21 Volts	94%
8 MHz 5 mm	22 Volts	No Data	100%
<b>Screen B</b>			
Transducer	Maximum Amplitude without Screen Present	Maximum Amplitude with Screen Present	Percent Decrease in Amplitude
4 MHz 5 mm	75 Volts	3 Volts	96%

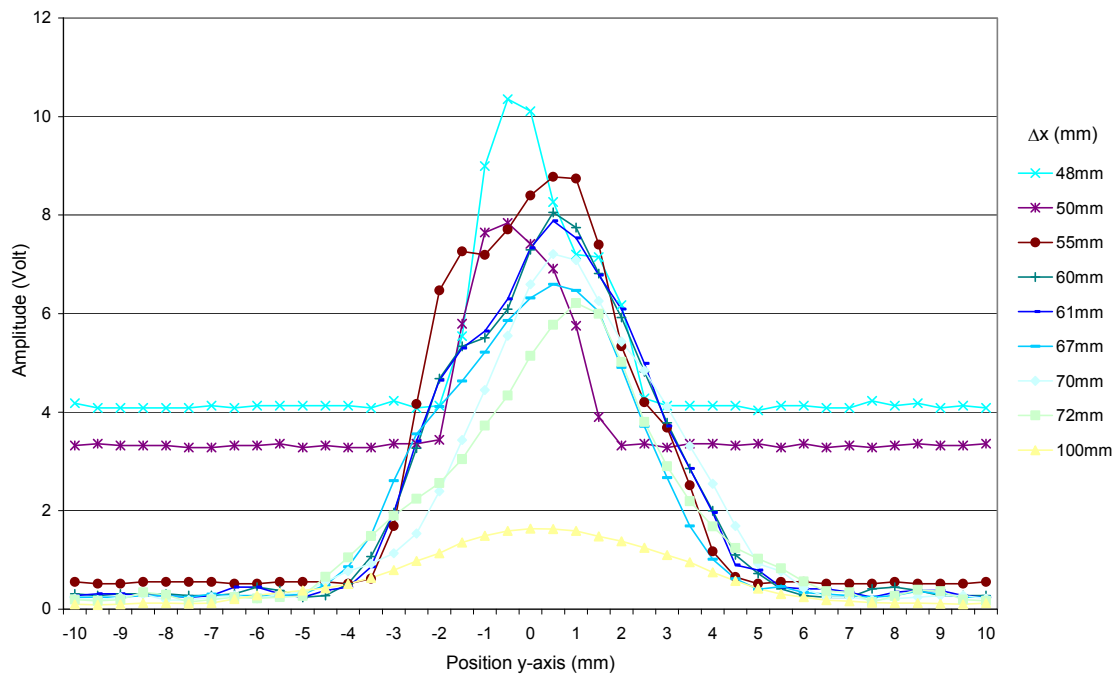


Figure 0-12: Echo Amplitude of 2 MHz 10mm Transducer with ScreenA at  $\Delta x = 40$  mm

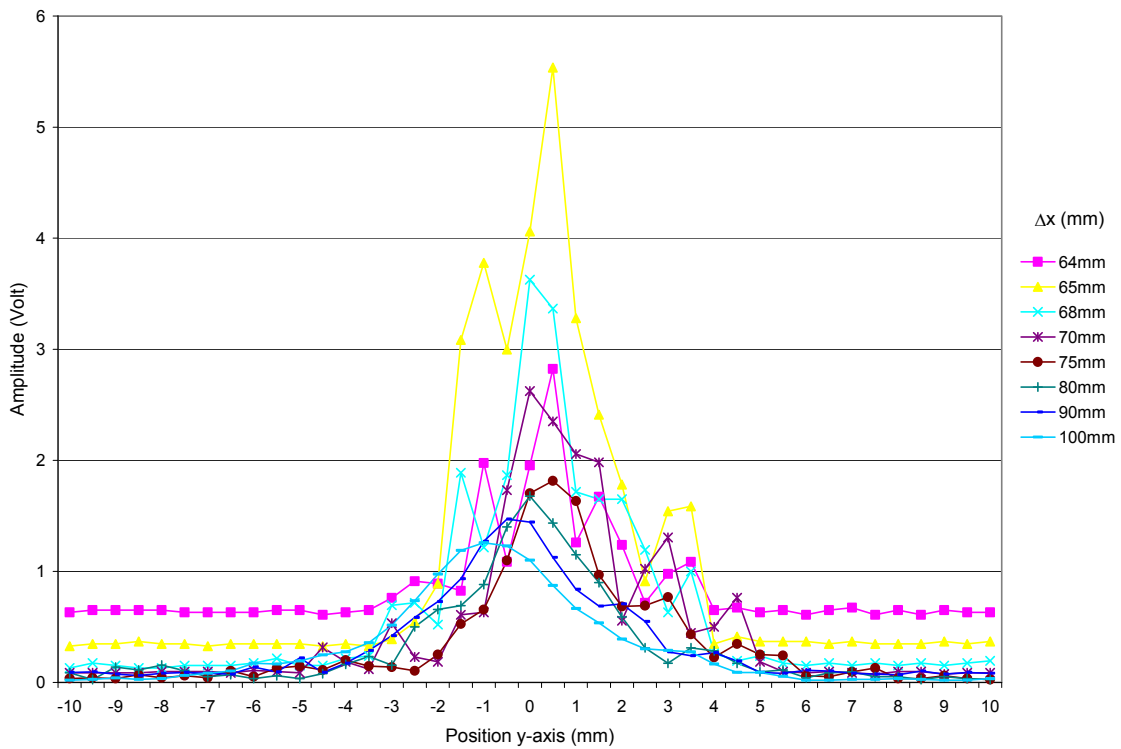


Figure 0-13: Echo Amplitude of 4 MHz 5 mm Transducer with ScreenA at  $\Delta x = 60$  mm

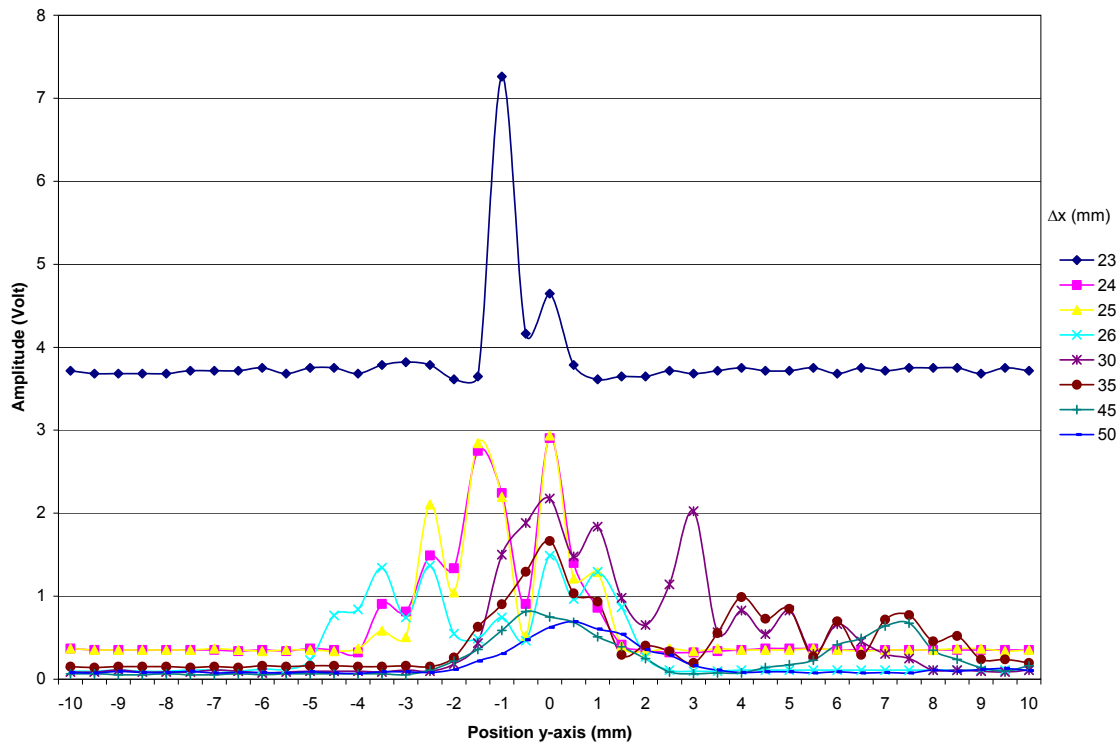


Figure 0-14: Echo Amplitude of 4 MHz 5 mm Transducer with ScreenB at  $\Delta x = 20$  mm

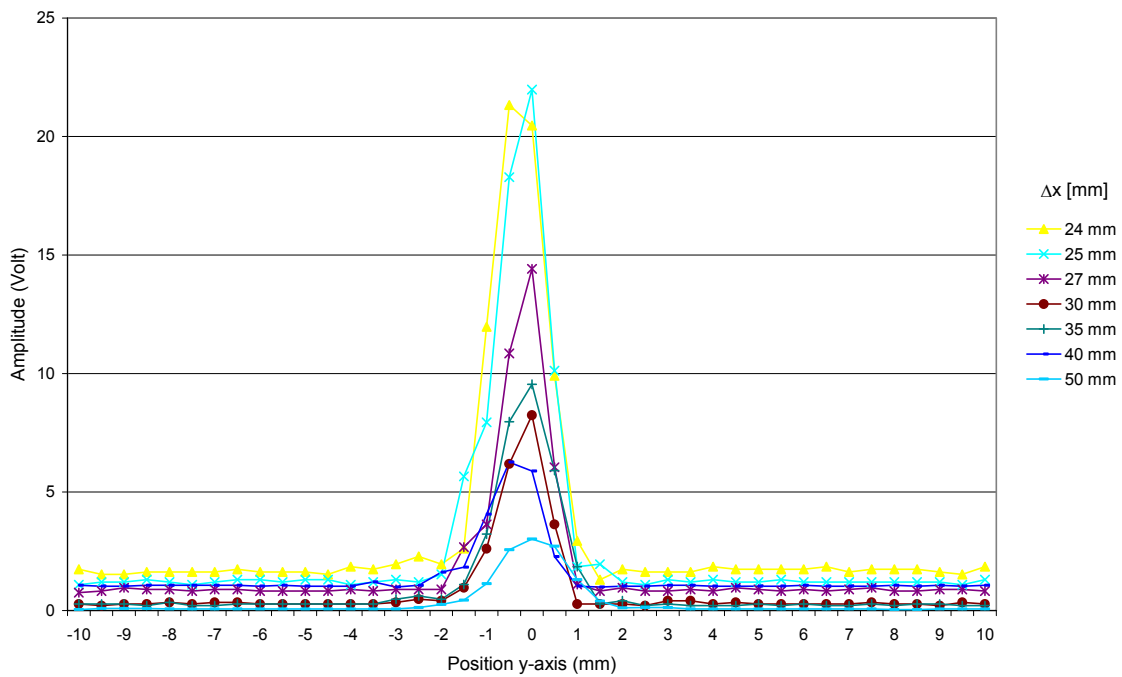


Figure 0-15: Echo Amplitude of 4 MHz 8 mm Focused Transducer with ScreenA at  $\Delta x = 20$  mm

As the echo amplitude decreases due to the presence of the forming screen, the gain of the system must be increased to achieve a measurable signal. As the gain of the system is increased, the ringing effect increases. This ringing effect causes the minimum measurable distance to increase. This is due to the fact that the region close to the forming screen is saturated. No measurements can be detected by the ultrasonic transducer in this saturated region. For the 2 MHz 10 mm transducer, the minimum measurable distance is 8mm. This is evident from the amplitude profile (Figure 0-12) and from the beam divergence profile (Figure 0-16). The closest that the small sphere could be placed to ScreenA before there was no detectable signal was 8 mm. Any attempt to place the sphere closer to the forming screen did not produce results because the signal received by the transducer was saturated. When the signal is saturated, the DOP 2000 system reads a very high (several orders of magnitude larger than the readings when the signal is not saturated) amplitude reading that is constant across the y-axis and a beam width of zero. While using the 4 MHz 5 mm and the 4 MHz 8 mm focused transducer, minimum measurement distances of 3 mm and 4 mm are achieved, respectively, for ScreenA. Again, these values were evident in the amplitude and beam divergence profiles as shown in Figure 0-13, Figure 0-15, Figure 0-17, and Figure 0-18. The 4 MHz 5 mm transducer also had a minimum measurement distance of 4 mm when ScreenB was in place as shown in Figure 0-14. After only one measurement with the 8 MHz 5 mm transducer, the ultrasonic signal diverged so much that no signal was detected by the device. This is shown in Figure 0-19. Due to high absorption and attenuation of the ultrasonic signal, when using the 8 MHz 5 mm transducer, no results were achieved when the forming screen is placed between the plastic sphere and the transducer. The closest distance from the plastic sphere to the screen over the widest range of transducer-screen-distances that produced detectable echoes was achieved with the 4 MHz 5 mm transducer. The 4 MHz transducer turned out to represent a good tradeoff between the high attenuation of the 8 MHz transducer and the low resolution (measurable depth and velocity) of the 2 MHz transducer.



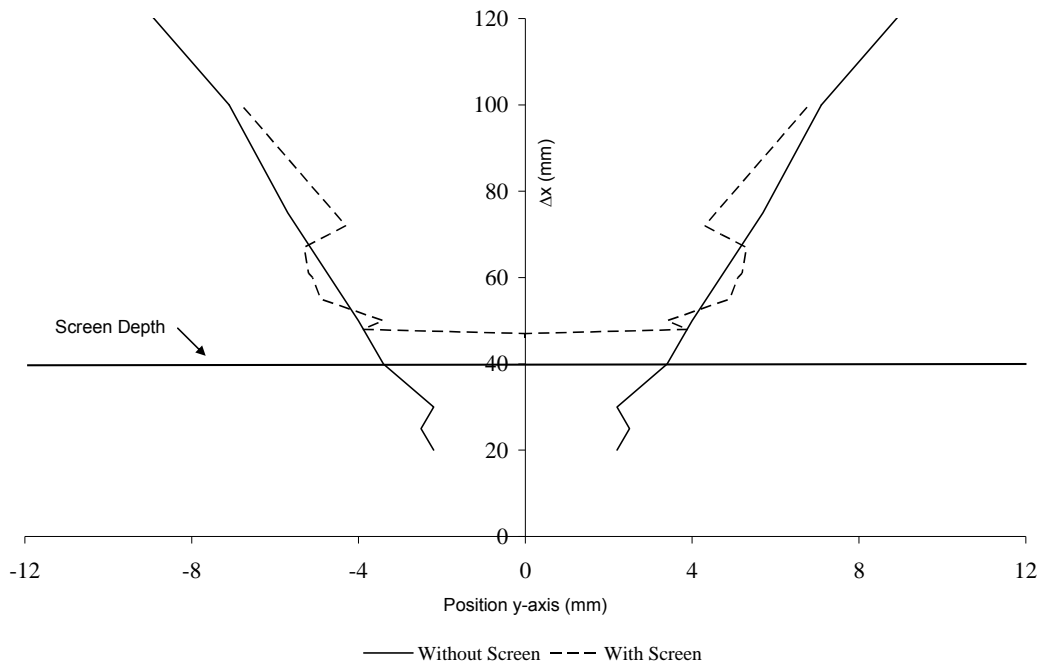


Figure 0-16: Beam Divergence Profile of 2 MHz 10 mm Transducer with ScreenA at  $\Delta x = 40$  mm (6 dB)

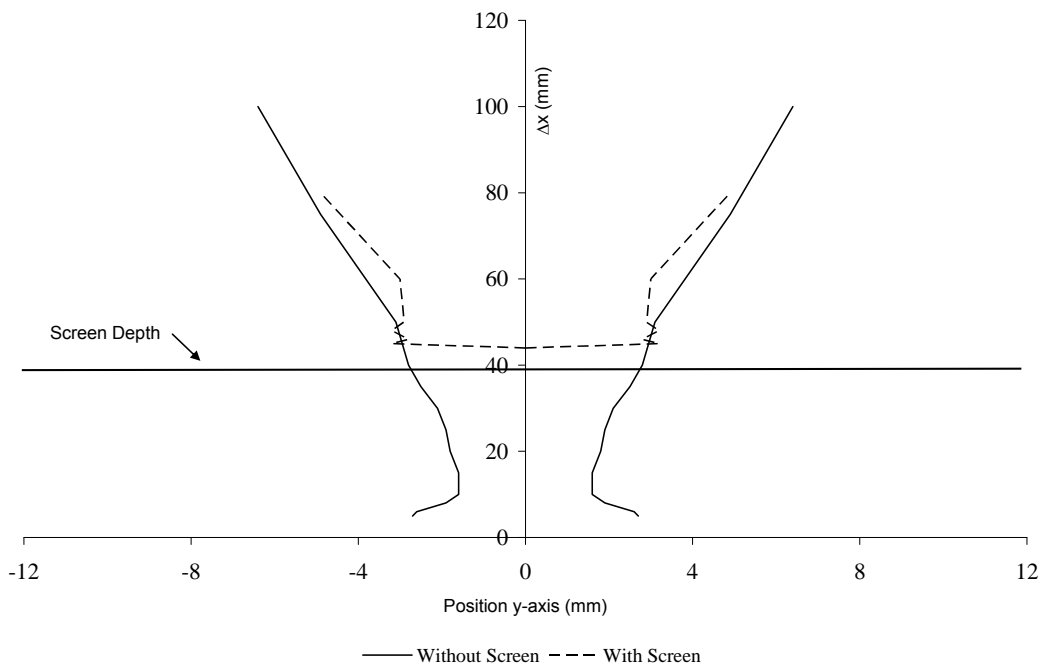


Figure 0-17: Beam Divergence Profile of 4 MHz 5 mm Transducer with ScreenA at  $\Delta x = 40$  mm (6 dB)

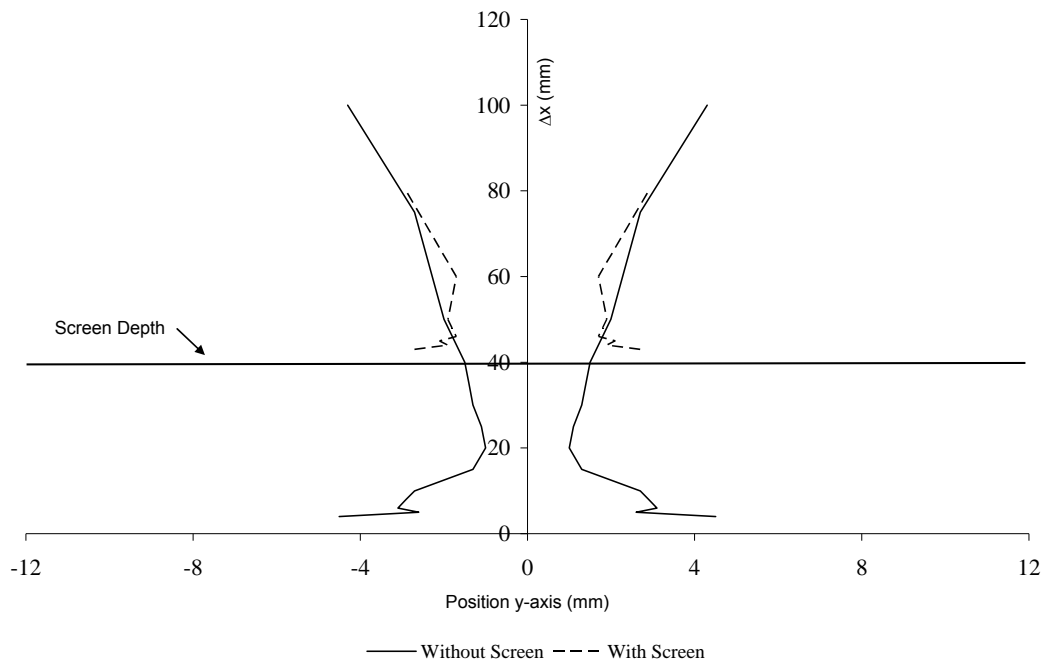


Figure 0-18: Beam Divergence Profile of 4 MHz 8 mm Focused Transducer with ScreenA at  $\Delta x = 40$  mm (6 dB)

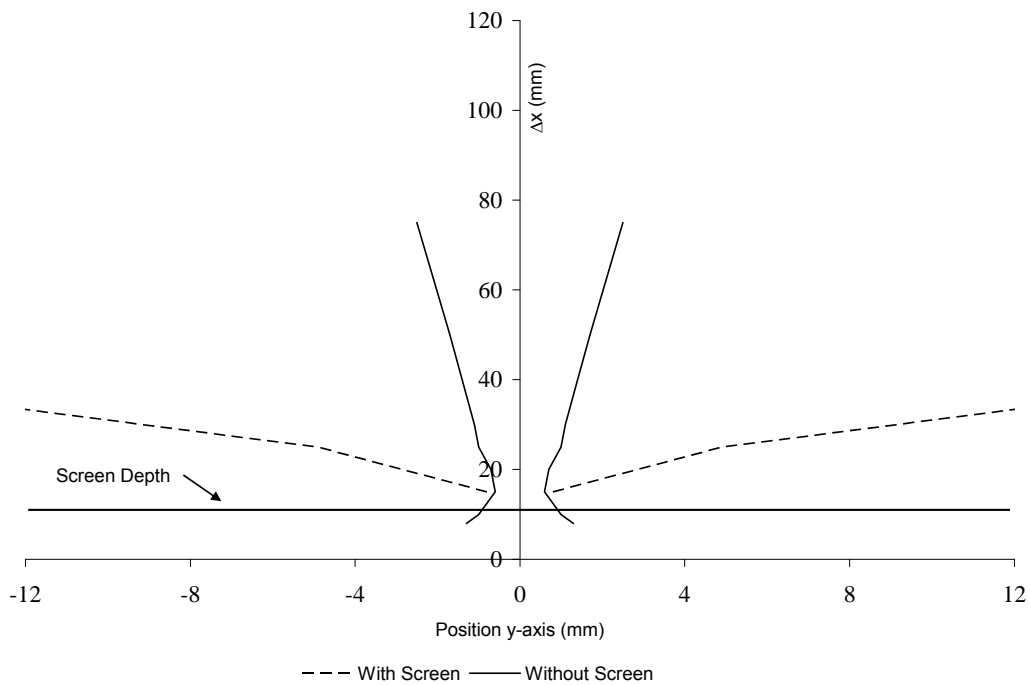


Figure 0-19: Beam Divergence Profile of 8 MHz 5 mm transducer with ScreenA at  $\Delta x = 10$  mm (6 dB)

The shape of the beam of the ultrasonic transducer changes when the screen is inserted in the field. When the screen is in place between the plastic sphere and the transducer, the beam seems to have two distinct regions. The “near screen field” is the region on the opposite side of the screen from the transducer, which is approximately 20-40 mm in length for the 2 MHz transducer and 20 mm in length for both of the 4 MHz transducers (focused and unfocused) with ScreenA. The “far screen field” is the region that is on the opposite side of the screen as the transducer and is past the “near screen field” (greater than 40 mm for the 2 MHz transducer and greater than 20 mm for the 4 MHz transducers) for ScreenA. In all cases (except for the 8 MHz transducer), the beam shape and width in the far screen field are very close to the same with and without ScreenA as shown in Figure 0-16, Figure 0-17, and Figure 0-18. In the near screen field, there is a common trend of beam convergence (narrowing of beam width) followed by beam divergence (widening of the beam width) as the beam progresses to the far screen field (Figure 0-16, Figure 0-17, and Figure 0-18). The beam width in the near screen field is slightly smaller (typically no more than 2mm) than the beam width when ScreenA is not present. The 3 dB divergence profiles are slightly narrower than the 6 dB divergence profiles in all cases. An example of a 3 dB beam divergence profile is shown in Figure 0-20 for the 4 MHz 5 mm transducer with ScreenA at  $\Delta x = 40$  mm.

The same trends for beam shape were apparent also when ScreenA was placed 20 mm away from the ultrasonic transducer. The ultrasonic beam converges slightly in the near screen field and then diverges as it passes into the far screen field. For the 4 MHz 8 mm focused transducer, the focal point without the screen is at 20mm, but with ScreenA placed 20 mm away from the transducer, the focal point shifts back approximately 10 mm as shown in Figure 0-21. This does not happen when ScreenA is at any other position that was tested with the 4 MHz focused transducer. Since the far screen field beam width and shape are very similar with and without the screen present, the angle of divergence for the transducers is similar in both cases. With ScreenA in place, the beam shape changes dramatically with different transducers so the trends are different for different transducers at different screen depths.

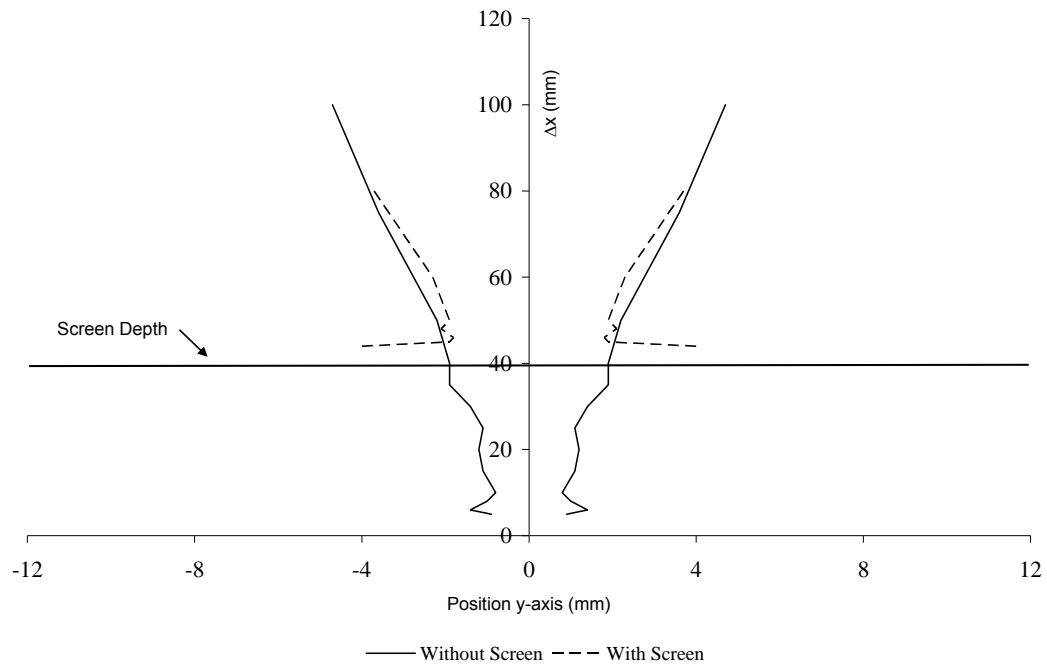


Figure 0-20: Beam Divergence Profile of 4 MHz 5 mm Transducer with ScreenA at  $\Delta x = 40$  mm (3 dB)

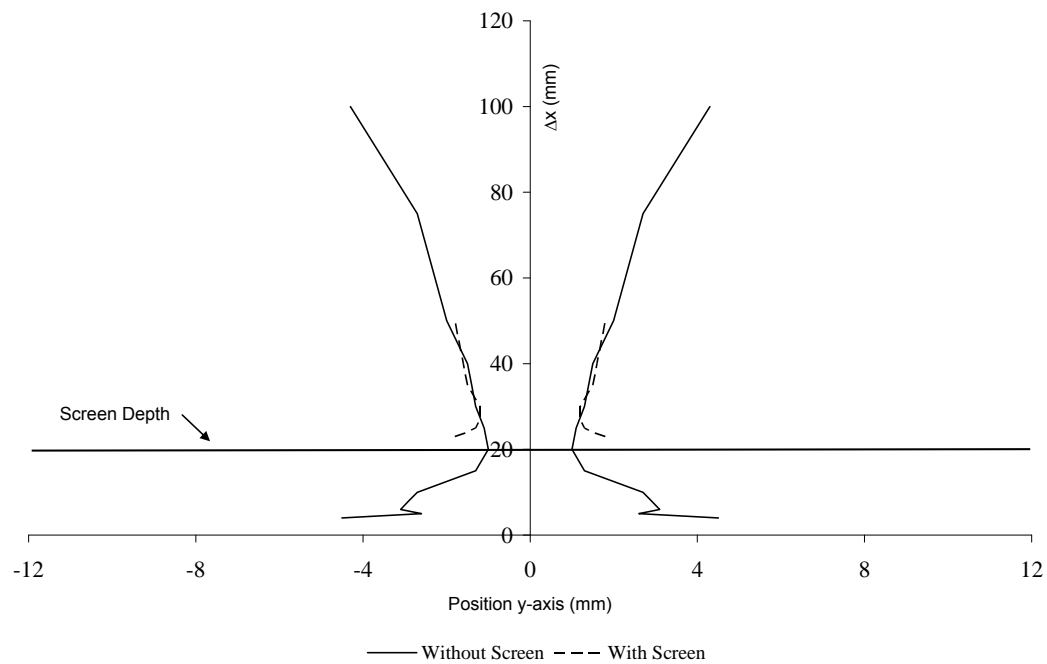


Figure 0-21: Beam Divergence Profile of 4 MHz 8 mm Focused Transducer with ScreenA at  $\Delta x = 20$  mm (6 dB)

## Modelling of Forming Screen

There are some numerical computations that allow the calculation of the absorption of acoustic energy due to the forming screen, and these would help verify the reduction of echo intensity due to the forming screen. In order to determine the reduction of echo intensity due to the forming screen, the acoustic impedance and the transmission coefficient of the forming screen must be determined. To calculate the acoustic impedance of the forming screen, several approaches were studied.

The first approach was to take the measured apparent density of the forming screen sample,  $1.18 \text{ g/cm}^3$ , and multiply it by the speed of sound in the forming screen,  $1700 \text{ m/s}$ , measured by Brodeur [8] to get a vague value of the acoustic impedance. This approach gives the acoustic impedance of the forming screen a value of  $2 \times 10^6 \text{ MKS Rayls}$ . No data was available for the speed of sound for the sample of forming screen used in this study.

The next approach was to try and use numerical models to come up with a value for acoustic impedance of the forming screen. Two numerical models were considered, the Delany-Bazley model which is a fundamental model in the area of sound propagation in fibrous materials and the Allard-Champoux model. The Delany-Bazley model predicted an acoustic impedance that was approximately the same magnitude as water. This would mean that the transmission coefficient was approximately 100% which is not at all realistic. The Allard-Champoux model gave similarly bad results that were not useful (transmission coefficient of  $\sim 100\%$ ). For reference, both models are described in Appendix C.

Due to the challenge in calculating the acoustic impedance of the forming screen with any reasonable accuracy, the reduction of echo intensity caused by placing the forming screen between the ultrasonic transducer and target sphere could not be calculated. One of the possible solutions of why the numerical results did not yield useful results is that the forming screen has a very high porosity, and the pores in the screen could be saturated with water (the test medium) rather than air. Unfortunately, the echo intensity reduction due to the forming screen for this study is solely based on the measured values using the pulsed ultrasonic Doppler system [25].

## Repeatability Tests

General trends such as beam convergence just past the forming screen and then divergence were seen throughout the forming screen tests, but all tests seemed to have some amount of variation. In the experimental setup of the forming screen tests, the forming screens were mounted in a Plexiglas mount that could be placed in the water bath with the transducer and the small plastic sphere. The forming screen sample was also much larger than the width of the ultrasonic beam emitted from the transducer at the depths that were tested. When placing the forming screen in the water bath, care was taken in each of the tests to have the screen at the same location for each test. The depth of the screen ( $\Delta x$  away from the transducer) was set each time by placing the plastic sphere in contact with the transducer and then backing it to the desired depth of the forming screen. The forming screen was then introduced into the water bath and placed in contact with the plastic sphere. The depth of the forming screen was then verified using the DOP 2000 ultrasonic system by means of visually inspecting at what depth the echo for the screen occurred. Using these two steps ensured that the forming screen was at the correct depth for every test. Once the depth of the forming screen was set, the screen could be moved laterally approximately 3 mm in either direction along the y-axis. Originally, it was thought that since the voids in the forming screen were so small, slight variation in lateral position would not affect the results of the beam shape measurements. As testing progressed, some questions of repeatability of the tests were raised due to the fact that although the general trends were the same for the beam shape measurements, the measurements themselves were significantly different for each test.

These concerns of repeatability of the measurements prompted a new set of tests that would determine if slight variations in the lateral position of the forming screen would produce different results for the beam shape measurements. Up to this point, the beam measurement tests had not been consecutively performed. Although the conditions were kept as close to the same as possible throughout the tests, there were slight variations in the tests including testing on different days, changing water in the water bath, and remounting the transducer between tests. The new set of

tests would all be done on the same day, in the same water bath (without changing the water), and with the ultrasonic transducer and plastic sphere mounted in the exact same positions for each test. The new tests were done with ScreenA and ScreenB. Since the most promising results in the tests leading up to these new tests had been with the 4 MHz 5 mm ultrasonic transducer, it was used for the new set of tests.

### ScreenA

For ScreenA, a total of nine different consecutive sets of data were taken. The first three sets of beam shape measurements (sets 1-3, black lines) were taken without moving anything except for the small plastic sphere (in order to generate slices of the beam field). The second three sets of data (sets 4-6, blue lines) were taken exactly the same as sets 1-3, but the screen was moved 0.5 mm laterally prior to the tests. The third three sets of data (sets 7-9, red lines) were taken with the exact same configuration as sets 4-6 (the previous sets) but waiting 2 hours after set 6 was taken. This last set of tests was meant to determine if the results of the beam shape measurements could be accurately repeated when nothing in the test setup changes. The same depths for the slices ( $\Delta x$  away from transducer) were used for all of the sets of data.

The 6 dB beam divergence profiles for sets 1-3 are presented in Figure 0-22. Set 2 shows a slight variation in beam width at  $\Delta x = 70$  mm, but otherwise, the beam widths for sets 1-3 are all within an average of 0.4 mm of each other for each measured slice. At  $\Delta x = 70$  mm the beam width of set 2 is 2.4 mm greater than the beam widths of sets 1 and 3. Figure 0-23 shows the beam divergence profiles for sets 4-6. Set 4 varies by 2.4 mm from sets 5 and 6 at  $\Delta x = 75$  mm. Sets 4-6 vary by only an average of 0.5 mm at all other measured slices. Figure 0-24 shows the beam divergence profiles for sets 7-9. Set 7 varies by 1.4 mm from sets 8 and 9 at  $\Delta x = 45$  mm and  $\Delta x = 75$  mm. The measured beam widths for sets 7-9 all average 0.6 mm for each other for each measured slice other than  $\Delta x = 45$  mm and  $\Delta x = 75$  mm.

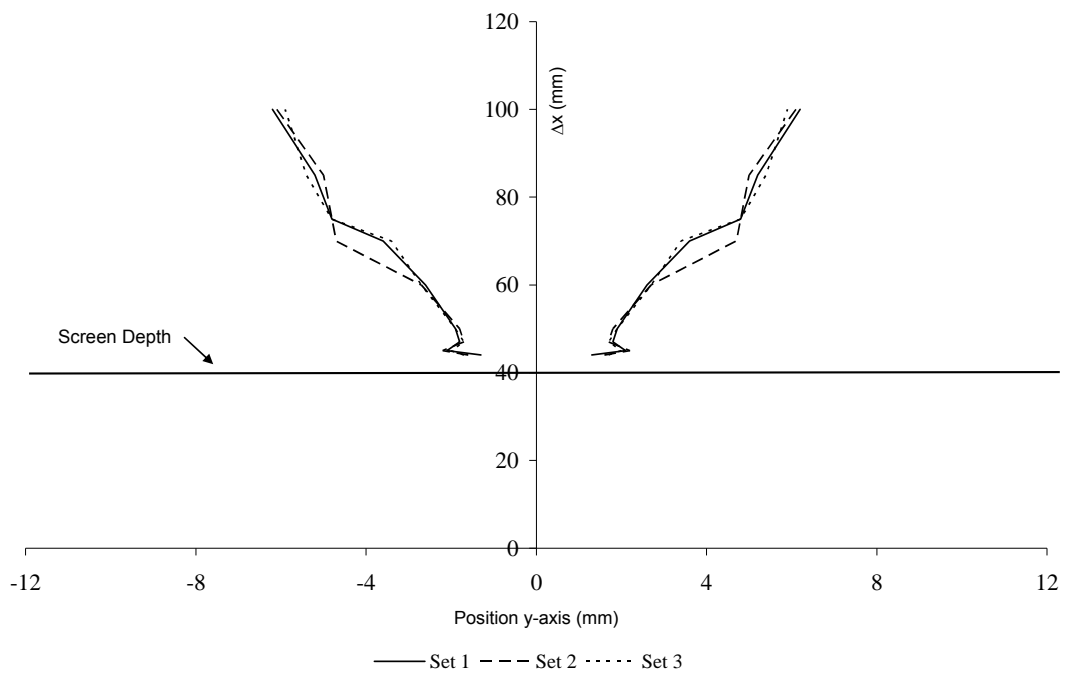


Figure 0-22: Beam Divergence Profile of 4 MHz with ScreenA at  $\Delta x = 40$  mm (6dB) Sets 1-3

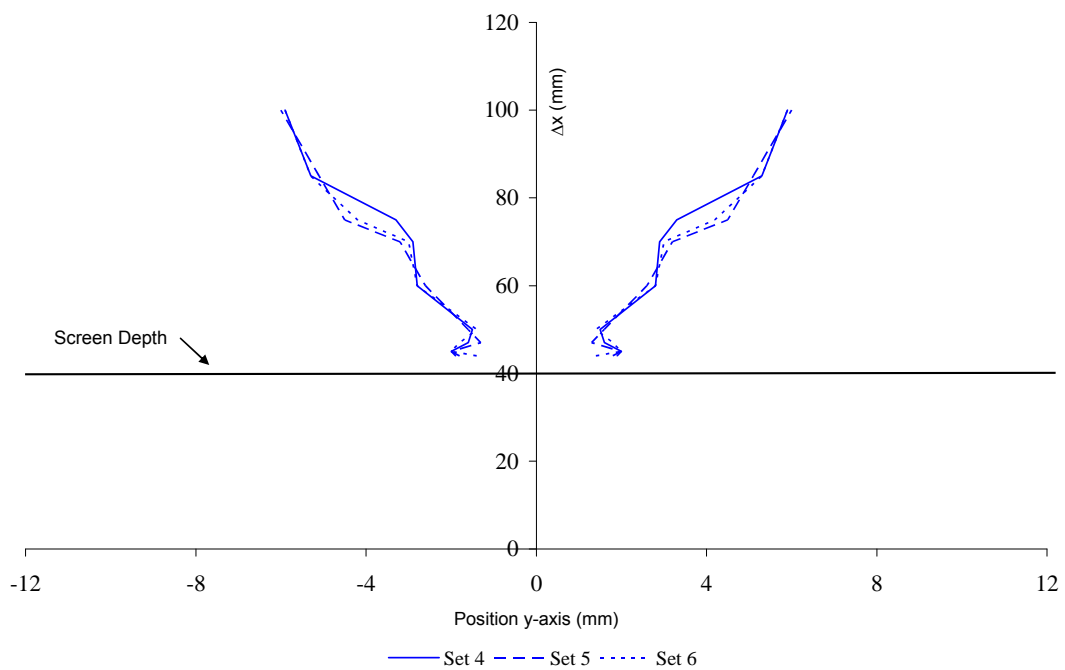


Figure 0-23: Beam Divergence Profile of 4 MHz with ScreenA at  $\Delta x = 40$  mm (6dB) Sets 4-6



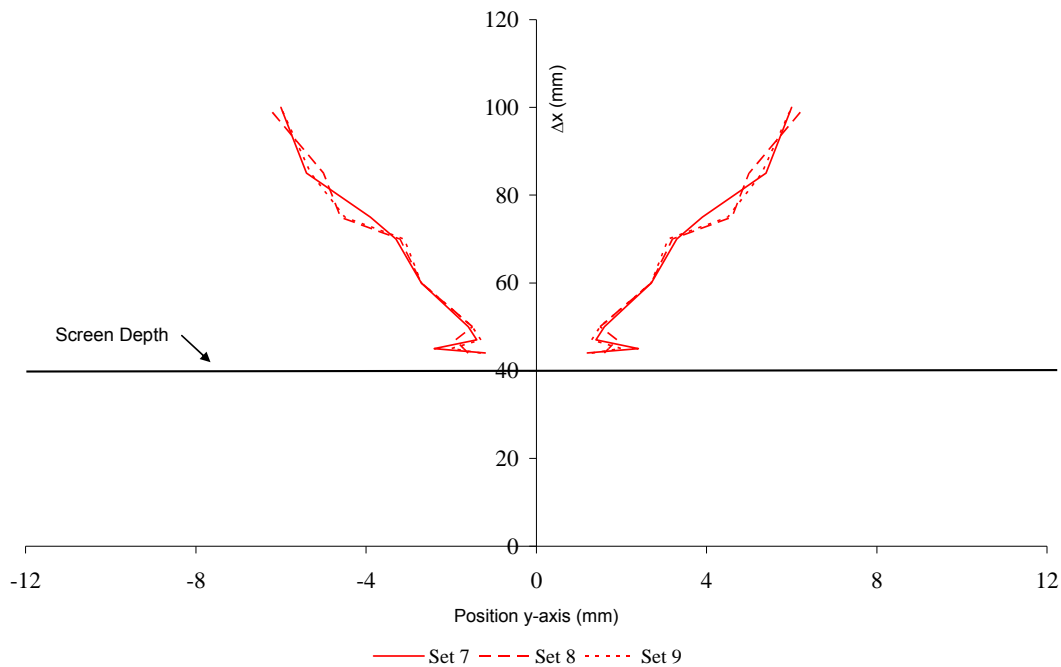


Figure 0-24: Beam Divergence Profile of 4 MHz with ScreenA at  $\Delta x = 40$  mm (6dB) Sets 7-9

The best way to check and see if the lateral movement of the forming screen caused variation in the beam shape measurements is to look at the relationship between sets 1-6 and sets 4-9. As previously stated, the only difference in the beam shape measurements between sets 1-3 and sets 4-6 was the change (by 0.5 mm) in lateral position (y-axis) of the forming screen. Figure 0-25 shows the beam divergence profiles for sets 1-6. The maximum difference in beam widths are 3.6 mm and 3.0 mm at  $\Delta x = 70$  mm and  $\Delta x = 75$  mm, respectively, for sets 1-6. The difference in measured beam widths for sets 1-6 average 0.8 mm for each measured slice other than  $\Delta x = 70$  mm and  $\Delta x = 75$  mm. The beam divergence profiles for sets 4-9 are shown in Figure 0-26. The maximum difference in beam widths is 2.6 mm at  $\Delta x = 75$  mm for sets 1-6. The difference in measured beam widths for sets 4-9 average 0.9 mm for each measured slice other than  $\Delta x = 75$  mm. Figure 0-27 shows sets 1-9 together on the same beam divergence profile. The maximum difference in the beam divergence measurements was 3.6 mm from sets 2 and 4 at  $\Delta x = 70$  mm.

Consequently, these two measurements were made when nothing in the experiment had changed except for the lateral screen position.

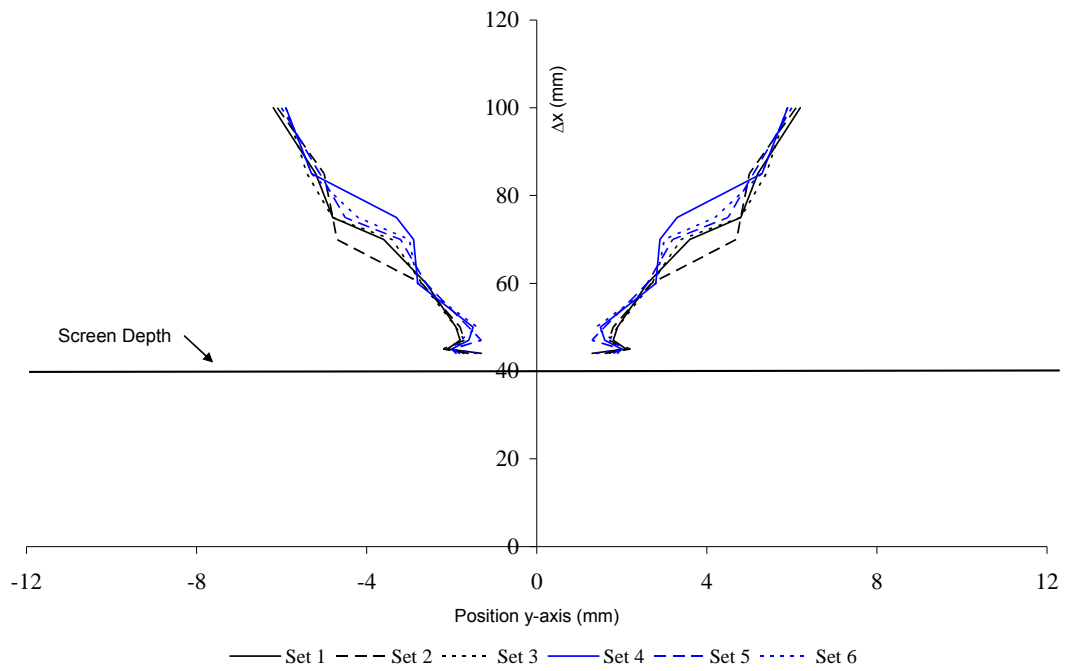


Figure 0-25: Beam Divergence Profile of 4 MHz with ScreenA at  $\Delta x = 40$  mm Set 1-6 (6dB)

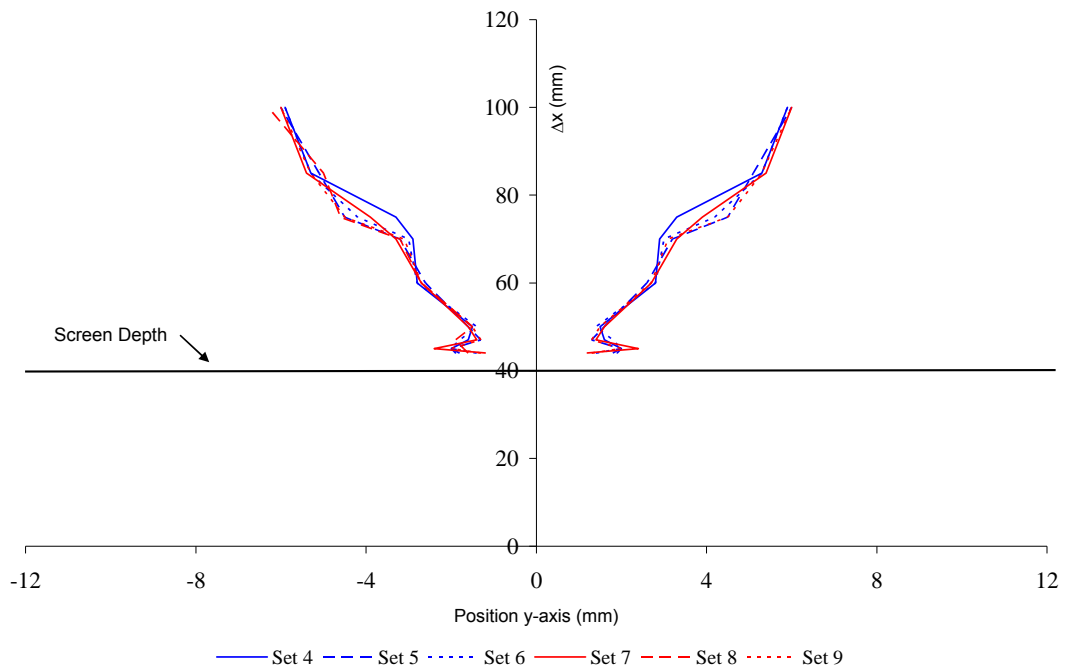


Figure 0-26: Beam Divergence Profile of 4 MHz with ScreenA at  $\Delta x = 40$  mm Set 4-9 (6dB)

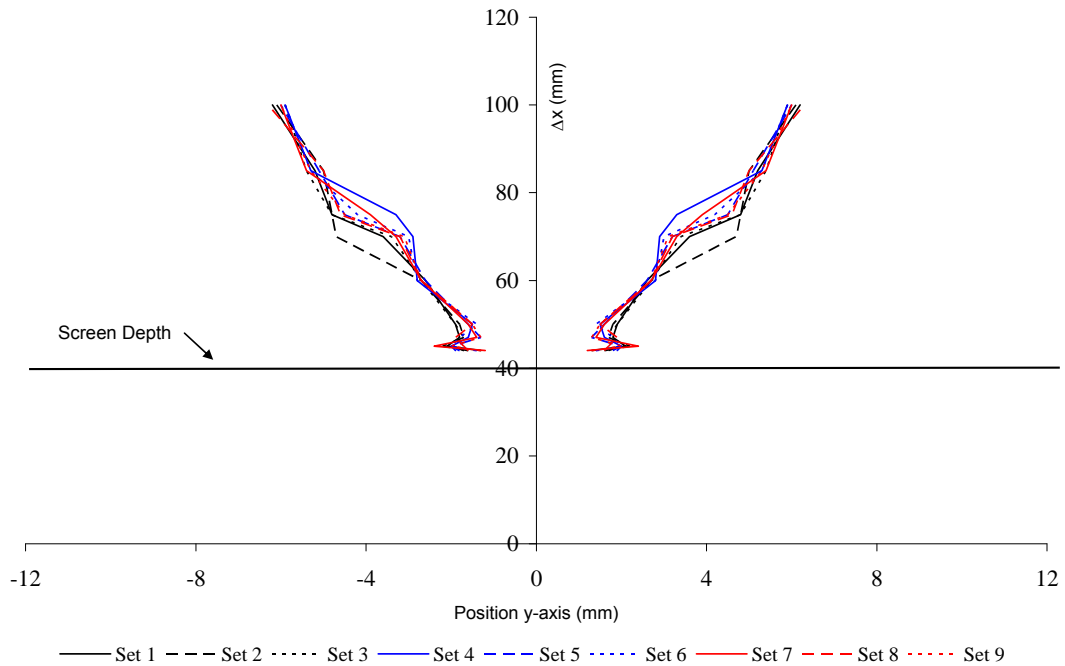


Figure 0-27: Beam Divergence Profile of 4 MHz with ScreenA at  $\Delta x = 40$  mm Set 1-9 (6dB)

## ScreenB

The same general procedure was applied to ScreenB with much more noticeable results. For ScreenB, a total of eight different consecutive sets of data were taken. Like ScreenA, the first three sets of beam shape measurements (sets 1-3, black lines) were taken without moving anything except for the small plastic sphere (in order to generate slices of the beam field). The second two sets of data (sets 4 and 5, blue lines) were taken exactly the same as sets 1-3, but the screen was moved 0.5 mm laterally prior to the tests. The third three sets of data (sets 6-8, red lines) were taken with the exact same configuration as sets 4 and 5 (the previous sets) but waiting 2 hours after set 5 was taken. Again, this last set of tests was meant to determine if the results of the beam shape measurements could be accurately repeated when nothing in the test setup changes, and the same depths for the slices ( $\Delta x$  away from transducer) were used for all of the sets of data.

Figure 0-28 shows the 6 dB beam divergence profile for sets 1-3 with ScreenB. This figure shows a beam divergence profile much different than the previous profiles generated for ScreenA. The most noticeable difference in the profile occurs with measurements made in the  $\Delta x = 70$  mm to  $\Delta x = 85$  mm region of the profile. When the DOP 2000 receives a saturated signal from the medium being measured, it typically returns a value of zero for the beam divergence width (the same as if the transducer was experiencing the ringing effect as mentioned in chapter 3). For sets 1 and 2, the DOP 2000 registered a value that was an order of magnitude greater and negative in value for the slice depth of  $\Delta x = 75$  mm. This is a discontinuity in the data due to a saturated region in the test medium and is analogous to the ringing effect. In set 3 the discontinuity in the saturated region is given a value of zero for the beam width. The general trend in this profile is a divergence of the ultrasonic beam from the screen to a depth of  $\Delta x = 60$  mm and then a slight convergence followed by another divergence of the ultrasonic beam at  $\Delta x = 85$  mm and beyond. At depths  $\Delta x = 44$  mm,  $\Delta x = 47$  mm, and  $\Delta x = 50$  mm, the beam widths vary by 3.4 mm for sets 1-3, but at all other depths (excluding  $\Delta x = 75$  mm), the beam widths vary by an average of 0.8 mm.

The 6 dB beam divergence profiles for sets 4 and 5 are presented in Figure 0-29. The greatest variation in beam width for these two sets is at  $\Delta x = 44$  mm and is 5.8 mm. The difference in beam widths for the other measured slices is an average of 0.6 mm. Figure 0-30 shows the beam divergence profile for sets 6-8. The greatest variation in beam width for these two sets is at  $\Delta x = 44$  mm and  $\Delta x = 45$  mm and is 5.2 mm. The difference in beam widths for sets 6-8 average 1.0 mm for other measured slices. Figure 0-29 and Figure 0-30 show the general trend of convergence of beam shape before divergence as the beam moves farther into the medium past the forming screen.

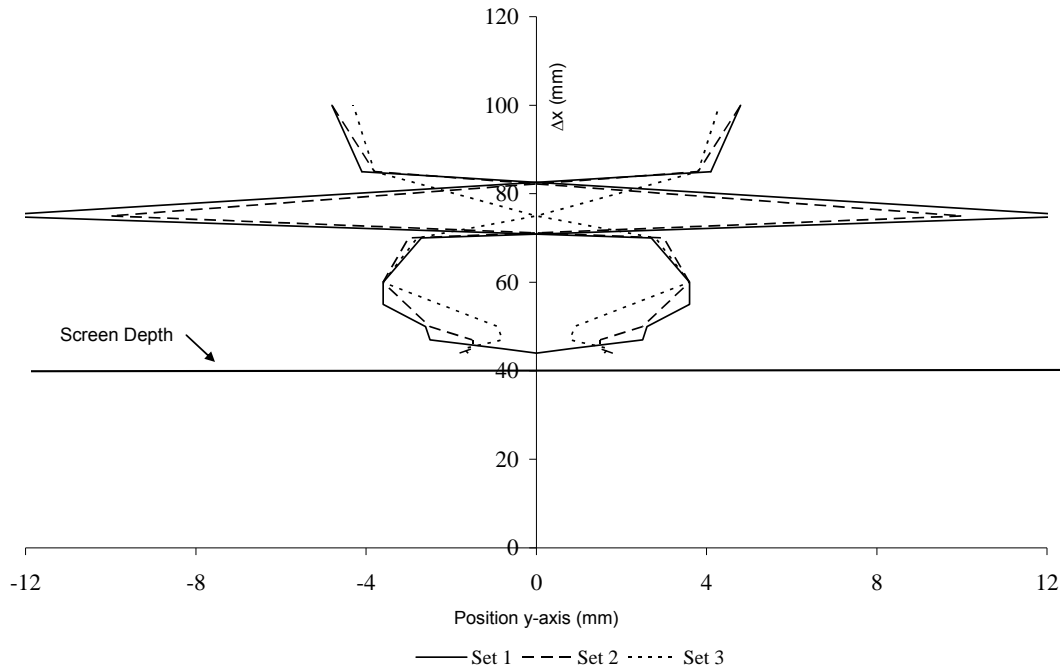


Figure 0-28: Beam Divergence Profile of 4 MHz with ScreenB at  $\Delta x = 40$  mm (6dB) Sets 1-3

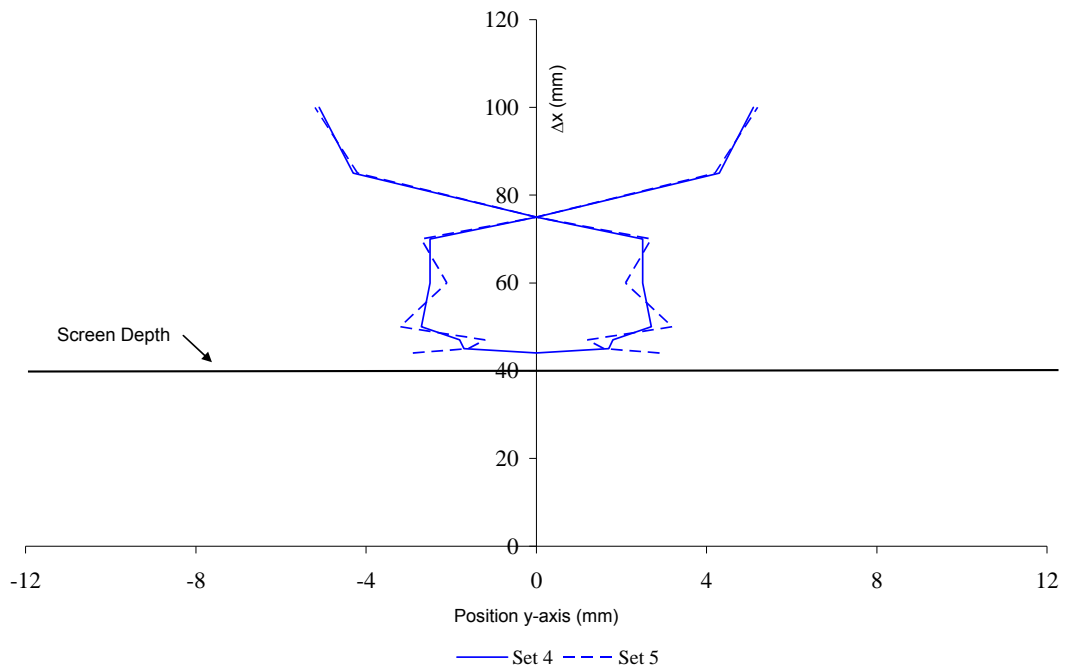


Figure 0-29: Beam Divergence Profile of 4 MHz with ScreenB at  $\Delta x = 40$  mm (6dB) Sets 5 and 6

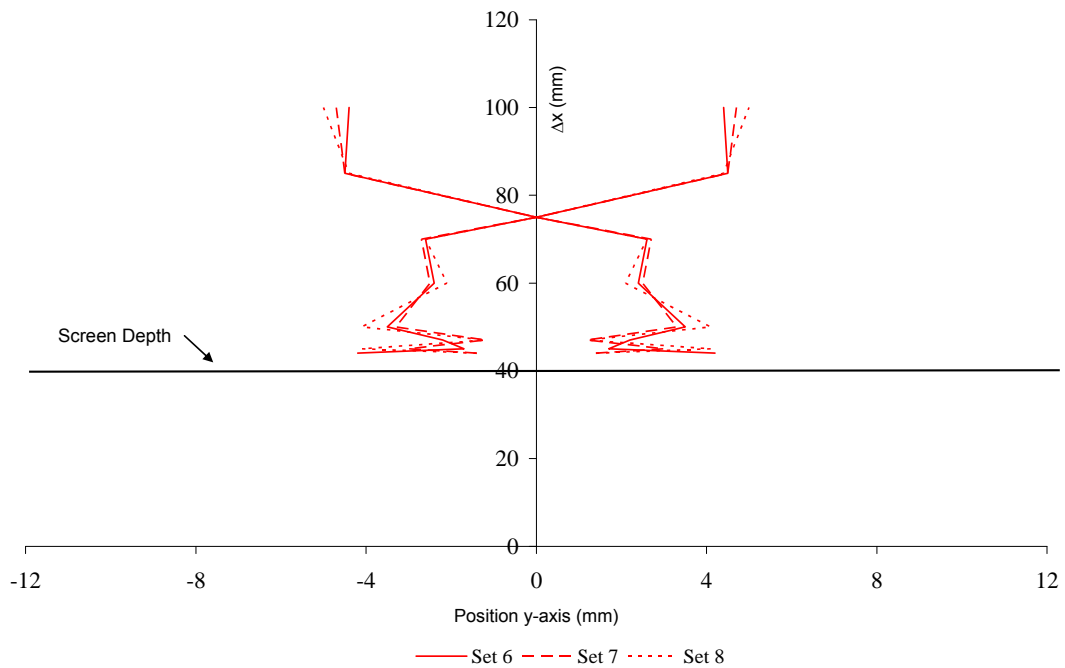


Figure 0-30: Beam Divergence Profiles of 4 MHz with ScreenB at  $\Delta x = 40$  mm (6dB) Sets 6-8

As with ScreenA, the changes that were made to the forming screen for the different sets of beam shape measurements can be studied for ScreenB. The main two data sets of interest are sets 1-5 and sets 4-8. The only difference in the beam shape measurements between sets 1-3 and sets 4 and 5 was the change (by 0.5 mm) in lateral position (y-axis) of the forming screen. Figure 0-31 shows the beam divergence profiles for sets 1-5. The maximum difference in beam width is 4.6 mm at  $\Delta x = 44$  mm and  $\Delta x = 50$  mm, but the difference in beam width for the different sets at all other measured slices averages 2 mm. The beam divergence profiles for sets 4-8 are shown in Figure 0-32. The maximum difference in beam width between the sets is 8.4 mm and 5 mm at  $\Delta x = 44$  mm and  $\Delta x = 45$  mm, respectively, and the average beam width difference for each of the other measured slices in the profiles is 1.2 mm. The 6 dB beam divergence profile for sets 1-8 with ScreenB is shown in Figure 0-33. The maximum difference in beam width is 6.6 mm between set 1 and set 8. The other sets average 2.8 mm in variation of beam width between measured slices.

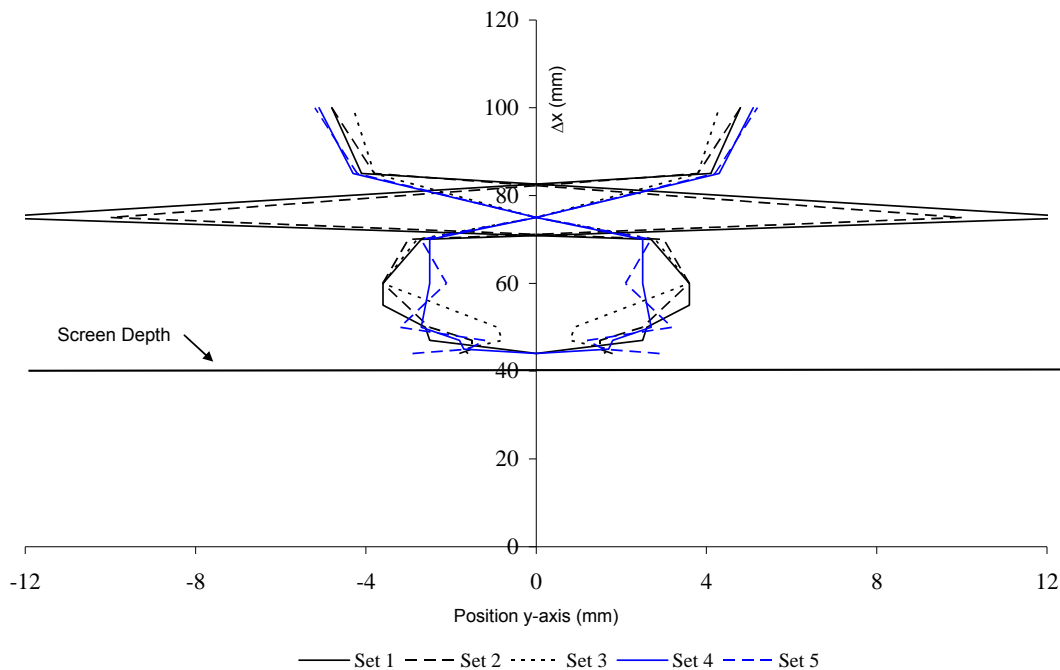


Figure 0-31: Beam Divergence Profiles of 4 MHz with ScreenB at  $\Delta x = 40$  mm (6dB) Sets 1-5

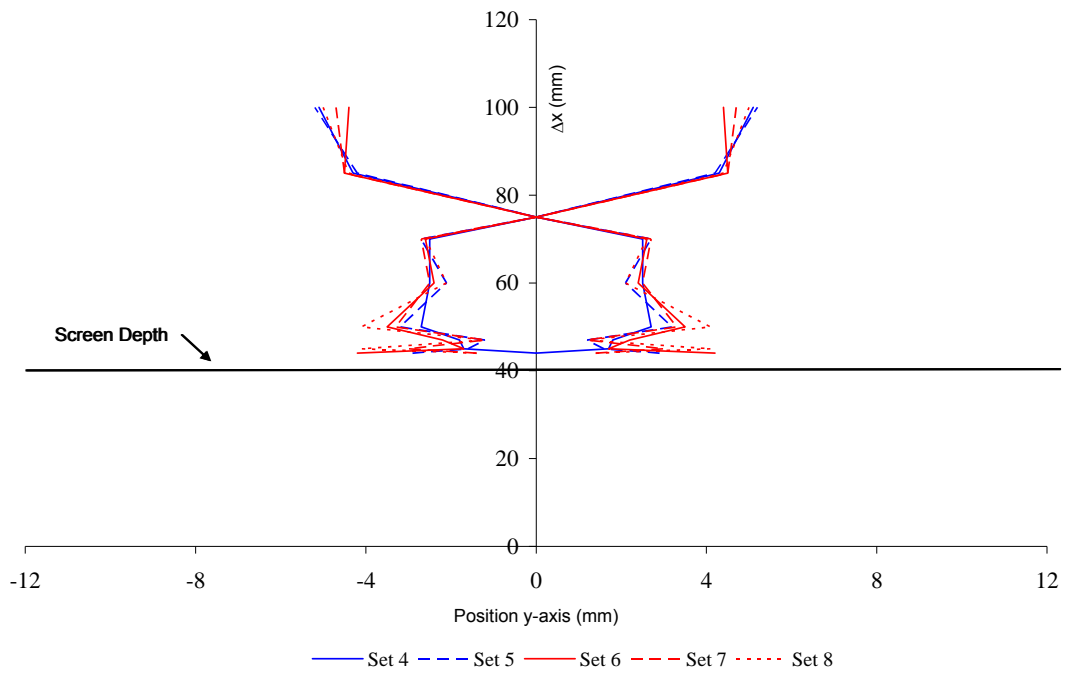


Figure 0-32: Beam Divergence Profiles of 4 MHz with ScreenB at  $\Delta x = 40$  mm (6dB) Sets 4-8

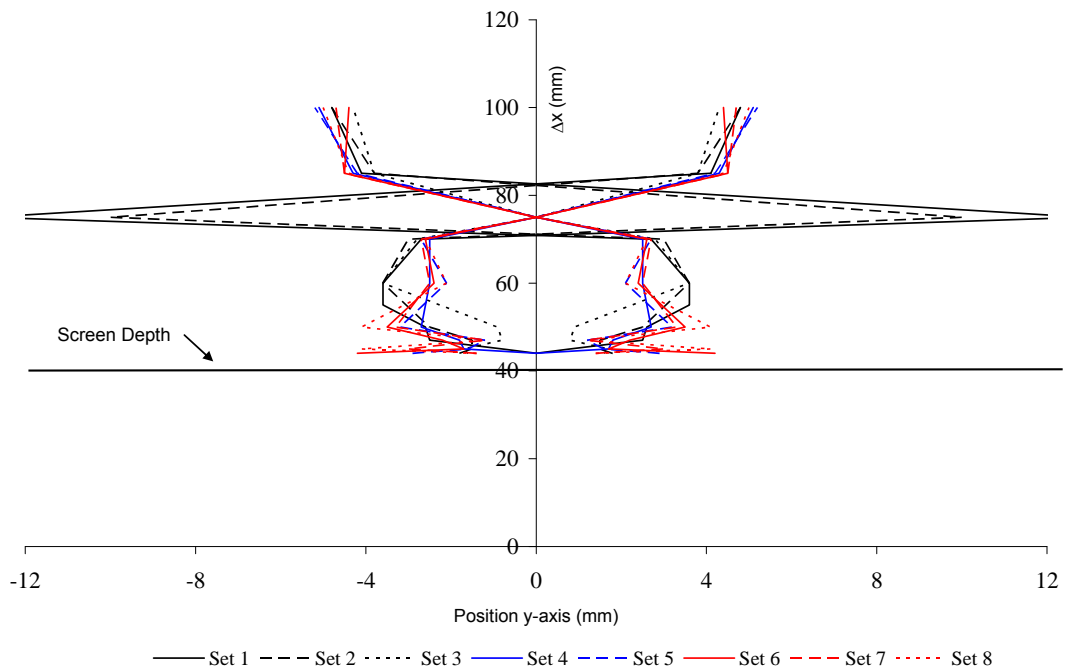


Figure 0-33: Beam Divergence Profiles of 4 MHz with ScreenB at  $\Delta x = 40$  mm (6dB) Sets 1-8



These tests with ScreenA and ScreenB show that there is more variation in beam width when the forming screen is moved laterally than when it is not moved. They also show that even though the pores in the forming screen are very small, they seem to have a great effect on the beam width measurements of the ultrasonic transducer. The greatest variation in the beam widths for ScreenA is at the depth  $\Delta x = 70$  mm. The greatest variation in the beam widths for ScreenB is very close to the forming screen, usually at  $\Delta x = 44$  mm, but there is also a large variation in beam width and a saturated region around  $\Delta x = 75$  mm. These depths are where the maximum variation in beam width is for each screen, but for both screens the largest variance in beam width between the sets is at  $\Delta x = 44$  mm and  $\Delta x = 70$  mm. It should be noted that beam width values for the discontinuity due to the saturated region in the test medium for ScreenB at  $\Delta x = 75$  were not included in the beam width analysis. This is because there was a discontinuity at this point in the measurements due to a saturated region in the test medium.